AFOSR-TR. 79-0180   LEVEL III   A006 234

(12)

AD A0 65617

Final Scientific Report
Contract Number F44620-74-C-0017

December 27, 1978

MECHANISMS OF MAGNETOPLASMADYNAMIC
ARCJEC ACCELERATION PROCESSES

Prepared for:

Air Force Office of Scientific Research/NA
Bldg.410
Bolling Air Force Base, D.C. 20332
Attn: Captain Marion R. Harrington

Prepared by:

Gordon L. Cann, PhD
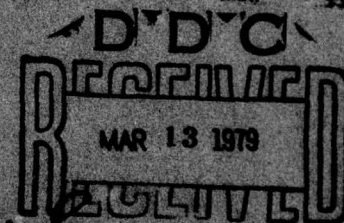President and Technical Director

Adriano C. Ducati
Consultant

TECHNION, INCORPORATED
17751 Sky Park East, Suite F
Irvine, California 92714

Approved:

Gordon L. Cann, PhD
President and Technical Director

D D C
RECEIVED
MAR 13 1979
C

79 03 12 033

Qualified requestors may obtain additional
copies from the Defense Documentation Center;
all others should apply to the National Technical
Information Service.

<u>CONDITIONS OF REPRODUCTION</u>

Reproduction, translation, publication, use and
disposal in whole or in part by or for the United
States Government is permitted.

Final Scientific Report
Contract Number F44620-74-C-0017

December 27, 1978

MECHANISMS OF MAGNETOPLASMADYNAMIC
ARCJEC ACCELERATION PROCESSES

Prepared for:

Air Force Office of Scientific Research/NA
Bldg.410
Bolling Air Force Base, D.C. 20332
Attn: Captain Marion R. Harrington

Prepared by:

Gordon L. Cann, PhD
President and Technical Director

Adriano C. Ducati
Consultant

TECHNION, INCORPORATED
17751 Sky Park East, Suite F
Irvine, California 92714

Approved:

Gordon L. Cann, PhD
President and Technical Director

APPROVED FOR PUBLIC RELEASE: DISTRIBUTION UNLIMITED.

REPORT DOCUMENTATION PAGE

READ INSTRUCTIONS
BEFORE COMPLETING FORM

1. REPORT NUMBER	2. GOVT ACCESSION NO.	3. RECIPIENT'S CATALOG NUMBER
AFOSR-TR. 79-0180		

4. TITLE (and Subtitle)	5. TYPE OF REPORT & PERIOD COVERED
MECHANISMS OF MAGNETOPLASMADYNAMIC ARCJET ACCELERATION PROCESSES.	FINAL rept. 15 Oct 73 – 30 Aug 78.
	6. PERFORMING ORG. REPORT NUMBER

7. AUTHOR(s)	8. CONTRACT OR GRANT NUMBER(s)
GORDON L CANN ADRIANO DUCATI	F44620-74-C-0017

9. PERFORMING ORGANIZATION NAME AND ADDRESS	10. PROGRAM ELEMENT, PROJECT, TASK AREA & WORK UNIT NUMBERS
TECHNION, INCORPORATED 17751 SKY PARK EAST, SUITE F IRVINE, CALIFORNIA 92714	2308C1 61102F

11. CONTROLLING OFFICE NAME AND ADDRESS	12. REPORT DATE
AIR FORCE OFFICE OF SCIENTIFIC RESEARCH/NA BLDG 410 BOLLING AIR FORCE BASE, D C 20332	Dec 78
	13. NUMBER OF PAGES 100

14. MONITORING AGENCY NAME & ADDRESS(if different from Controlling Office)	15. SECURITY CLASS. (of this report)
	UNCLASSIFIED
	15a. DECLASSIFICATION/DOWNGRADING SCHEDULE

16. DISTRIBUTION STATEMENT (of this Report)

Approved for public release; distribution unlimited.

17. DISTRIBUTION STATEMENT (of the abstract entered in Block 20, if different from Report)

18. SUPPLEMENTARY NOTES

19. KEY WORDS (Continue on reverse side if necessary and identify by block number)

PLASMA ACCELERATION; SATELLITE PROPULSION; SPACE CHARGE LIMITED
ION FLOW; ELECTROSTATIC NOZZLES.

20. ABSTRACT (Continue on reverse side if necessary and identify by block number)

Investigations into methods of utilizing ambient gas as propellant at satellite altitudes have been experimentally and analytically investigated. As part of this investigation, a class of space charge limited plasma accelerators has been studied. Experimentally, discharges in these devices are low current (.1 amp to 2 amps) and high voltage (200v to 10,000v). Ions are produced by electron bombardment of the adsorbed gases on the anode. Treating the flow of ions and electrons as a conducting fluid permits analogies with fluid flow phenomena. Sub- and supercritical flow for both ions and electrons correspond to subsonic

DD FORM 1473
1 JAN 73

391 204

79 03 12 033

and supersonic flow in a fluid. In one-dimensional flow, the electric field creates an "electrostatic nozzle" with critical flow occurring where the electric field is zero (the "electrostatic throat") A rigorous analysis of the flow gives qualitative agreement with measured discharge characteristics. Space charge buildup limits the ratio of beam power to electric power input to under 1% for the operating mode wherein ions are produced from the adsorbed gas on the anode. Conventional performance as a pulsed plasma accelerator can be obtained by desorbing the gas from the anode rapidly so that breakdown occurs.

TABLE OF CONTENTS

TABLE OF CONTENTS (continued)

LIST OF FIGURES

LIST OF FIGURES (continued)

ABSTRACT

Investigations into methods of utilizing ambient gas
as propellant at satellite altitudes have been experimentally and
analytically investigated. As part of this investigation, a
class of space charge limited plasma accelerators has been studied.
Experimentally, discharges in these devices are low current
(.1 amp to 2 amps) and high voltage (200v to 10,000v) . Ions
are produced by electron bombardment of the adsorbed gases on
the anode. Treating the flow of ions and electrons as a conducting
fluid permits analogies with fluid flow phenomena. Sub- and
supercritical flow for both ions and electrons correspond to sub-
sonic and supersonic flow in a fluid. In one-dimensional flow,
the electric field creates an "electrostatic nozzle" with critical
flow occurring where the electric field is zero (the "electro-
static throat"). A rigorous analysis of the flow gives quali-
tative agreement with measured discharge characteristics. Space
charge buildup limits the ratio of beam power to electric power
input to under 1% for the operating mode wherein ions are
produced from the adsorbed gas on the anode. Conventional
performance as a pulsed plasma accelerator can be obtained by
desorbing the gas from the anode rapidly so that breakdown occurs.

1.0   INTRODUCTION

The thrust to conduct the maneuvers associated with
satellite reorientation, orbit modification and drag make-up
has up to the present been provided by any one of a number of
means:

> cold gas jets
>
> hydrazine jets
>
> ion engines
>
> arc jets and plasma thrusters carrying
> their own propellant
>
> chemical rocket propulsion systems
>
> colloid thrusters.

The problems and disadvantages of these systems are many
and diverse, but they have in common the critical problem that
the total impulse available is proportional to the mass of
propellant carried on the space craft. Mission life-times must
hence be programmed from the point of view of this limitation,
rather than from the mission requirements. Utilization of ambient
atmosphere as propellant eliminates this problem.

Studies have been conducted to determine the feasibility
of collecting air at high altitudes for use in chemical or
electrical propulsion systems. The most extensive investigations
were those of S. T. Demetriades and colleagues on the Air-Scooping
Orbital Rocket (A-SCOR) (Ref. 1-4). Similar studies were carried
out elsehwere (Ref. 5-9). These studies indicated that the system
was feasible provided that a power source of considerable size
(several Megawatts) was available to assist in the collection
process and to heat the air (thermally or electrically) used as
propellant in the thruster system. The lack of an adequate
power source appears to be the main obstacle to the imple-
mentation of this system.

The ideal propulsion system for satellites would be one for which both power and propellant were available in situ. Rapid improvements in solar cell technology and in the technology of axisymmetric plasma accelerators over the past ten years make it desirable at this time to investigate the feasibility of such a truly infinite total impulse propulsion system. Obviously, unless extremely large solar cell arrays are utilized (on the order of square kilometers), the power level available will be low (under 10 kilowatts), so that the cryogenic collection and storage of propellant - as suggested in the above-mentioned studies - will not be feasible. An alternate means of propellant handling could result through the use of a space-electric ram jet. The postulated space-electric ram jet would utilize an axisymmetric electric discharge surrounded by a solenoidal magnetic field to ionize and/or accelerate the ambient air. When the power is supplied by solar cells this type of propulsion system has the potential for extremely large total impulses.

The space-electric ram jet can be postulated to operate in a number of modes. The mode employed can depend upon many factors, such as power availability, thruster performance characteristics, possible communications interference, etc. One possible mode of operation that would appear to be very efficient would be operation of the thruster at altitudes where the ambient ionization level is near its peak, i.e. in the region between 200 and 300 km altitude. By properly designing the magnetic field configuration, the discharge could perhaps encompass a large cross-section in space and utilize only the existing ions and electrons. In this manner the thrust would be produced without any accompanying ionization energy loss. Also, in this mode, it might be possible to operate with a high electric potential across the electrodes and hence obtain high specific impulses (over 3000 sec).

Unfortunately, laboratory experiments to investigate if such an operational mode is feasible are far beyond the scope of the present investigation. In fact, it is likely that the only practical test of this hypothetical mode of operation would be a test in near space on an orbiting laboratory, such as that envisioned for the space shuttle.

A steady-state operating mode for a space-electric ram jet has been observed in laboratory experiments at pressure levels of over 10^{-3} Torr. (Ref. 10-18). It remains to be seen if this mode of operation, which requires volume ionization, will perform well at pressure levels of 10^{-7} to 10^{-3} Torr. Part of the current may be carried in a "filament" (which can be many centimeters in diameter) that extends out from the cathode and loops back to the anode. This loop encompasses all of the magnetic flux lines inside the anode ring. The "loop" current rotates rapidly (200-800khz) and, because of the high electron concentration and temperature within it, acts as an ionization front, ionizing the atoms of the ambient gas as it spins through them. The ions that are produced are then accelerated (electrostatically) toward the axis and join with electrons from the cathode jet to form the exahust beam that escapes from the magnetic field and produces a net axial thrust and a torque on the engine. It is also possible to consider that the thrust is produced by $j \times B$ forces, in which case the axial thrust results from the interaction of the azimuthal current with the radial component of the applied magnetic field.

The distance that the current loop extends out into the space behind the engine would probably depend upon the ambient pressure, the applied magnetic field strength, and the total current. In some cases (very low pressures) it may be many meters long and several meters in diameter at its widest.

Such an engine would produce a torque as well as a thrust.

In order to have no torque on the average, the magnetic field would be reversed periodically. Naturally, use could be made of the torque for spinning or despinning the vehicle.

It should be emphasized that the discharge modes postulated above are very different from conventional vacuum arcs (Ref. 19). In the latter, the material which forms the plasma and exhaust beam is almost invariably eroded from the cathode or, less frequently, from the anode, or insulator structure. Great care would have to be taken in the design of space-electric ram jet devices to ensure that this does not occur and that the major component of the discharge plasma and exhaust beam consists of air.

A quite different operational mode can be postulated. This would be a pulsed mode which utilizes the air adsorbed on the surfaces of the engine. A discharge can be postulated to ionize and accelerate this adsorbed air off the surface and shape it into an exhaust beam. The surface would then be free to adsorb more air from the atmosphere and the cycle could be repeated.

Of the three operational modes postulated above, the last is the one that lends itself most readily to experimental investigation in the laboratory. Extensive tests have, accordingly, been conducted on several engine configurations that operated in this mode.

Results from these tests have been reported in references (19 and 20). These results will be examined in detail in this report from two points of view. First, the experimental data will be compared to theoretical performance estimates. Second, the experimental data will be used to generate thruster performance estimates.

2.0 ENGINE CONFIGURATION AND OPERATIONAL CHARACTERISTICS

Detailed descriptions of the measurements made on the various discharge and accelerator configurations tested can be found in references. For convenience this information is summarized here.

2.1 Assembly 1.

A special piece of test equipment was designed and constructed for investigating the influence upon the discharge characteristics of desorption effects on the electrode surfaces of an axisymmetric plasma accelerator. A picture of this device is shown in Figure 1. It consists of 2 NRC ionization gauges (type 807) facing each other and connected together by a glass cylinder two inches in diameter and seven inches long. A glass cylinder three inches in diameter and twelve inches long is connected to this assembly to increase the volume. A Veeco ionization gauge is connected to the system for measuring pressure. This whole assembly was mounted in a furnace and connected to a vacuum pumping system. The system was baked at a temperature of about 350°C for several days while it was evacuated to a pressure of under 10^{-7} Torr at which time it was sealed off. The volume of assembly 1, is 2.56 litres (156 cubic inches).

One of the NRC tubes was used an as axisymmetric plasma accelerator. This was accomplished by using the cylindrical collector plate as an anode and the heated filament as the cathode. The grid was allowed to float electrically. A coil of 300 turns of number 18 wire was wound around the outside of the gauge to produce a solenoidal magnetic field. This coil was two inches long, had an I. D. of two inches and an O. D. of four inches. The coil was calibrated

5

and found to produce 32.5 gauss per ampere of current on the center line.

The filament was heated by discharging a 60,000 μ. f. condenser bank through it. The bank could be charged to several hundred volts, but it was found that charging it to voltages of 25 to 31 volts provided adquate heating. The scope traces shown in Figure 2 show the current through the filament and the thermal radiation from the filament as measured by a photo cell, both as a function of time. It is seen that the peak filament temperature is attained about 60 milli-seconds after the current through the filament is initiated. One side of the filament was grounded.

The magnet coil was energized by another 60,000 μ. f. condenser bank. The scope trace in Figure 3 shows both the current through the magnet coil and the current through the filament as a function of time. The magnetic field strength has a time constant for decay of about 70 milli-seconds.

Energy for the discharge between the ring anode and the heated filament was supplied from a condenser charged to a high voltage. Tests have been conducted with condenser banks of 2, 4 and 32 μ. f. charged to voltages of from 1,000 volts to 8,000 volts.

The other NRC ionization gauge was used as an ion detector. The circuit shown in Figure 4 was used. The differential amplifier was used so that both electrodes of the probe could be left floating to ensure that no current flowed between the discharge tube and the ion detector.

2.1.1. Summary of Experimental Results Using Assembly 1.

Over 500 independent tests were conducted with this piece of equipment. A unique type of slow discharge has been

6

observed in this device. Typical current-voltage traces
from an oscilloscope are shown in Figure 5. At high voltages
(over 8,000 volts) and high ambient pressure (over 10^{-4} Torr)
breakdown occurred and a more conventional arc discharge
resulted. The peak current in the "slow"discharge was usually
a fraction of an ampere and the discharge lasted tens of
milli-seconds. The current transistioned discontinuously
(in less than 2 μ. sec.) to a much lower value as the potential
drop across the electrodes reached some low, critical value
(≈ 1,200 volts).

2.1.1.1 Influence of Ambient Pressure

It was possible to reduce the pressure in the assembly
to 1 x 10^{-8} Torr by using the Veeco ionization gauge as an
ion pump for a period of several days. Also, by heating up
the grid of the Veeco gauge as well as the tube it was possible
to raise the pressure in the assembly to 10^{-3} Torr. Tests
were hence conducted over a pressure range of 10^{-3} to 10^{-8}
Torr.

No magnetic field was applied. The filament condenser
bank was charged to 30 volts and a 4 μ. f. condenser was
charged to 4,000 V for the discharge. Current and voltage traces
were recorded as a function of time using an oscilloscope. (Fig. 5)
Negligible changes in the discharge characteristics occurred
as the pressure was raised from 3 x 10^{-8} Torr to 5 x 10^{-5} Torr.
From this pressure on, however, as the pressure was increased
the following trends were observed:

- the peak current increased with the pressure.
- the magnitude of the discontinuous current change increased.
- the voltage drop at which the discontinuous current change occurred decreased as the pressure was increased.

7

The magnitudes of these changes are shown in the following table.

Pressure	Peak Current Amps	Discontinuous Current Change Amps	Voltage Drop at Discontinuity Volts
3×10^{-8}	.6	.20	1900
5×10^{-5}	.6	.20	1900
1×10^{-4}	.65	.20	1800
3×10^{-4}	.98	.45	1200
7×10^{-4}	1.20	1.2	400

2.1.1.2 Influence of Charging Voltage on 4 μ. f. Discharge Capacitor

A series of tests were conducted in which the pressure was held constant at 3.5×10^{-6} Torr. No "discharge" occurred until the charging potential was over 1200 volts. Increasing the voltage on the capacitor beyond this point increased both the peak current and the duration of the current. Characteristic current-voltage relationships are plotted in Figure

2.1.1.3 Influence of Size of Discharge Capacitor

Many tests were conducted with a 16 μ. f. capacitor charged to 4000 volts. In general, the peak current was only slightly higher than when a 4 μ.f. was used. The time duration of the discharge was, however, 5-6 times as long. In some cases the current discontinuity was observed, and in others not. The discharge lasted long enough so that the heating current through the filament had decayed to a small fraction of its peak value. Since at times the voltage on the discharge capacitor did not fall below 3000 volts, it can be concluded that there is not sufficient ion bombardment of the cathode to sustain the discharge.

2.1.1.4 Influence of an Applied Solenoidal Magnetic Field

When a solenoidal magnetic field was applied to the discharge a number of effects were observed. The discharge current decreased as the magnetic field was increased and was eventually suppressed completely at field strengths of several thousand gauss. Oscillations in the discharge current occurred at moderate magnetic field strengths (several hundred gauss) at a frequency of about 1,000 hz.

A very interesting interaction between the cathode emission and the magnetic field was observed. The magnet coil was excited simultaneously with the filament current and a peak magnetic field of about 1,350 gauss occurred after a few milli-seconds. The energy to heat the filament was then decreased successively for each test point. The discharge current rose as this happened and the oscillations died out. At a quite low energizing energy for the filament the discharge current was eventually suppressed.

2.2 Assembly 2

Because of the small volume of Assembly 1 a strong possibility existed that some interaction could occur between the discharge and the walls of the vessel. Also, the chamber was so small that no accurate measurement of a time of flight could be made to obtain some estimate of the particle velocity in the exhaust beam. Accordingly, a series of tests were planned and conducted in a large volume facility, using the same engine configuration as in the earlier tests and covering the same range of operation parameters.

A vacuum chamber located at the Convair Aerospace Division of General Dynamics in San Diego was used for the tests. The specifications for the chamber "A" are given in Table I. Because of the time and cost involved in pumping down and repressurizing the chamber, it was decided to accomplish as many tests as possible with only one pumpdown. This required that special precautions be taken to ensure that no malfunction of any part of the electrical or mechanical equipment in the tank could occur. Duplicate engines were mounted in the tank and four ion detectors were positioned downstream of the source. The placement of these components are shown in Figure 6. A photograph

10

of the duplicate source (engine) is shown in Figure 7. The ion detectors were all identical and a photograph of one is shown in Figure 8.

A great deal of care was taken to maintain the noise level in the detector circuits at a very low level. All electrical connections between the tank and the instrumentation were made with #8 shielded amphenol cable. A special feed-through plate was designed and constructed which ensured that shielding continued through the tank walls and also that no ground loops could occur in the tank. A photograph of the feed-thru plate is shown in Figure 9.

All of the electrical and diagnostic equipment needed for the test was assembled in a mobile laboratory from which all tests were conducted on the site. A schematic of the electric circuit for the ion source (engine) is shown in Figure 10. All the shields for the cables, the chassis and the instrumentation were grounded on a common bus inside the mobile laboratory to minimize ground loop effects.

The circuits for the ion detectors were designed to measure accurately picoamperes of beam current impinging on the detector faces. The circuits used are shown schematically in Figure 11. The detector consisted of a thin wall outer cylindrical nickel electrode 3 cm in diameter by 2 cm long and a central solid copper electrode 1 cm in diameter and 2 cm long. These electrodes were rigidly mounted in a plexiglass plate and the electrical connections to the leads were buried in the plexiglass. The polarity was such that the outer electrode would collect ions and the inner one of the electrons.

Note: Throughout the testing period the test environment was kept at liquid nitrogen temperature.

2.2.1 Summary of Experimental Results Using Assembly 2

During a period of 3 days over 300 data points were taken. A discharge, similar to that observed in Assembly 1, was observed. Breakdown occurred much more readily, however, hence most of the tests were conducted with the discharge capacitor charged to only 2000 volts.

2.2.1.1 Influence of Ambient Pressure

Data was taken on the discharge characteristics and probe signals as the tank pressure was bled up. During these tests a standard "accelerator" operating condition was used, where a peak solenoidal magnetic field of several hundred gauss occurred in the region of the electrodes. No significant change in the discharge characteristics was observed over the pressure range of 1×10^{-6} Torr up to 3×10^{-5} Torr. At higher pressures high frequency oscillations were observed and the peak current decreased.

These oscillations were measured on the detectors as well as across the discharge. The magnitude of the discontinuous change in the current remained constant, but the potential drop at which the discontinuity occurred decreased as the pressure was increased above 3×10^{-5} Torr.

2.2.1.2 Influence of Changing Voltage on 4 μ.f. Discharge Capacitor

A series of tests were conducted at the minimum pressure obtainable near the beginning of the test series. The voltage on the discharge capacitor was increased in increments of 500 volts, starting at 1000 volts. The peak current increased rapidly with the initial voltage across the discharge; however, the time duration of the discharge increased only marginally. Breakdown occurred intermittently

when the charging potential was over 2500 volts. Discharge characteristics are displayed in Figure 12.

2.2.1.3 Influence of an Applied Solenoidal Magnetic Field

As the solenoidal magnetic field strenth was increased, the peak current of the discharge decreased. The time duration of the discharge increased with the magnetic field. At modestly high magnetic field strengths, oscillations occurred in the current and voltage of the discharge. Increasing the magnetic field strength eventually led to a breakdown.

2.3   Discussion of Experimental Results

The insensitivity of the "slow" discharge characteristics to the ambient pressure leads to the conclusion that the discharge is associated with ions produced on the anode surface due to electron bombardment. Examination of the discharge curves also leads to the conclusion that the processes are dominated by space charge effects.

The measured signals on the detectors in the experiments on Assembly 2 indicate that plasma has been accelerated downstream of the discharge. Two approaches towards estimating the performance potential of the device as a space propulsion system become available:

i) attempt to measure the thrust, the mass flow rate and the electrical power, or alternatively the impulse,the mass utilized per pulse and the electrical energy. Use these measured quantities to calculate the specific impulse and the efficiency of the device.

ii)   identify the mechanisms and processes from
      the experimental results and construct a
      theoretical model to predict performance
      capabilities.

Past history of plasma propulsion studies indicates
that approach (i) can often lead to over-optimistic
performance estimates due to the difficulty of the measure-
ments and to interactions occurring between the engine and
the test environment. Where feasible, then, approach (ii)
has much to recommend it. The flow of non-colliding
charged particles can be accurately modelled and a well
defined boundary value problem can be formulated and
solved. This approach was hence taken and the analysis of
the charged particle flow (treated as a continuum) is
presented in the next section.

3.0   ANALYSIS

The flow of a completely ionized plasma with or without currents needs to be investigated in order to determine the magnitude of the ion and electron flux rates in the projected engine configurations. It is appropriate to examine the flow in the limit when no volume collisions between the ions and electrons occur. This is a problem that has been studied by numerous investigators, starting with Langmuir. The innovation attempted here is to utilize the fluid flow equations.

In order to gain some understanding of the procedure and of the significance of the results, the problem is investigated in three phases:

    Phase I   one-dimensional ion or electron
               flow - the classical Langmuir-
               Childs problem.

    Phase II   one-dimensional ion and electron
               flow. Each species flow constitutes
               a current.

    Phase III quasi-one-dimensional flow of ions
               and electrons.

3.1   PHASE I   ONE DIMENSIONAL EQUATIONS FOR ELECTRON OR ION FLOW

Mass conservation:

$$|e| n w = - j = \text{constant.} \qquad 3.1.1$$

Momentum conservation:

$$-E = \frac{m}{|e|} u \frac{du}{dx} + \frac{1}{|e| n} \frac{dp}{dx} \qquad 3.1.2$$

Energy conservation:

$$-E = \frac{m}{|e|} u \frac{du}{dx} + \frac{m}{|e|} \frac{dh}{dx} \qquad 3.1.3$$

Poisson's Equation:

$$\frac{dE}{dx} = \frac{|e| n}{\varepsilon_o} \qquad 3.1.4$$

Equation of State:

$$p = n k T \qquad 3.1.5$$

THERMODYNAMIC AND GASDYNAMIC RELATIONS
FROM MOMENTUM AND ENERGY CONSERVATION

$$\frac{1}{|e|n} \, dp = \frac{m}{|e|} \, dh$$

becomes $\left(\dfrac{p}{p_c}\right) = \left(\dfrac{h}{h_c}\right)^{\frac{\gamma}{\gamma-1}}$ 3.1.6

From equation of state

$$\left(\frac{n}{n_c}\right) = \left(\frac{h}{h_c}\right)^{\frac{1}{\gamma-1}}$$ 3.1.7

From continuity

$$\left(\frac{u_c}{u}\right) = \left(\frac{h}{h_c}\right)^{\frac{1}{\gamma-1}}$$ 3.1.8

or $\dfrac{u}{u_c} = \left(\dfrac{h_c}{h}\right)^{\frac{1}{\gamma-1}}$

17

WORKING EQUATIONS

Introduce (8) into (3)

$$\frac{du}{dx} = \frac{\frac{|e|}{m} E}{\frac{(\gamma-1) h_c}{u_c} \left(\frac{u_c}{u}\right)^\gamma - u} \qquad 3.1.9$$

Introduce (1) into (4)

$$\frac{dE}{dx} = -\frac{|j|}{\varepsilon_0 u} \qquad 3.1.10$$

Multiply (10) by E and
Introduce (9) into (10)

$$\frac{|e|}{m} E \frac{dE}{dx} = \frac{|j|}{\varepsilon_0} \left[1 - \frac{(\gamma-1) h_c}{u_c u} \left(\frac{u_c}{u}\right)^\gamma \right] \frac{du}{dx} \qquad 3.1.11$$

Equations (9) and (11), together with boundary
conditions permit a complete solution to the
problem.

SOLUTION FOR $h_c = 0$ (Langmuir-Childs Solution)

Boundary Conditions:

$u_c = 0$

$E_c = 0$

$V_c = 0$

Integration of eq. (9) gives:

$$\frac{u^2}{2} = \frac{|e|}{m} V \qquad\qquad 3.1.12$$

Integration of eq. (11) gives:

$$E = -\sqrt{\frac{2m|j|}{|e|\,\varepsilon_o} u} \qquad\qquad 3.1.13$$

Combining eq. (12) and (13) and integrating again

$$\frac{4}{3} V^{3/4} = \sqrt{\frac{2m}{|e|}\frac{|j|}{\varepsilon_o}} \sqrt{\frac{2|e|}{m}} \; x$$

Rewriting in conventional form

$$\boxed{|j| = \frac{4}{9} \frac{\varepsilon_o}{x_A^2} \sqrt{\frac{2|e|}{m}} \; V_a^{\,3/2}} \qquad\qquad 3.1.14$$

19

GENERAL SOLUTION

1) Eq. (9) indicates that for u to increase monatonically with x the electric field must be positive for $u < u_{cr}$ and negative for $u > u_{cr}$.

Where

$$u_{cr}^{\gamma+1} = a_c^2 \, u_c^{\gamma-1}$$

or

$$\boxed{\frac{u_{cr}}{a_c} = \left(\frac{u_c}{a_c}\right)^{\frac{\gamma-1}{\gamma+1}}} \qquad 3.1.15$$

2)

When

$$u = u_{cr}$$
$$E = 0 \qquad\qquad 3.1.16$$

3) Define $\dfrac{u}{u_{cr}} = M$, then $u_{cr} = a_c \, M_c^{\frac{\gamma-1}{2}}$ $\qquad$ 3.1.17

4) Rewrite equations (9) and (11)

$$\frac{dM}{dx} = \frac{\dfrac{|e|E}{m\ u_{cr}^2}}{\dfrac{1}{M^\gamma} - M}$$ 3.1.9a

$$\frac{d}{dx}\ \frac{E^2}{2} = \frac{m|j|\ u_{cr}}{|e|\ \varepsilon_o}\left(1 - \frac{1}{M^{\gamma+1}}\right)\ \frac{dM}{dx}$$ 3.1.11a

5) Integrate (11a) from the critical point to an arbitrary point.

$$E = \pm\ \sqrt{\frac{2m|j|\ u_{cr}}{|e|\ \varepsilon_o}\left[M + \frac{1}{\gamma M^\gamma} - \frac{\gamma+1}{\gamma}\right]}$$ 3.1.18

21

6) Introduce E into (9a).

$$\frac{dM}{dx} = \sqrt{\frac{2|e||j|}{\varepsilon_0 m u_{cr}^3}} \quad \frac{M + \frac{1}{M^2} - \frac{\gamma+1}{\gamma}}{\left| M - \frac{1}{M^2} \right|} \qquad 3.1.19$$

using eq. 17 and introducing a non-dimensional space variable ξ, an equation that can be evaluated in terms of the conditions at the cathode is obtained.

$$\xi = \sqrt{\frac{2|e|^2 M_c}{\varepsilon_0 m a_c^2}} \; x \qquad 3.1.20$$

$$\frac{dM}{d\xi} = M_c^{\frac{2-\gamma}{2}} \quad \frac{M + \frac{1}{\gamma M^\gamma} - \frac{\gamma+1}{\gamma}}{\left| M - \frac{1}{M^\gamma} \right|} \qquad 3.1.21$$

for $\gamma = 5/3$

$$\frac{dM}{d\xi} = M_c^{1/6} \quad \frac{M + \frac{5}{3M^{5/3}} - \frac{8}{5}}{\left| M - \frac{1}{M^{5/3}} \right|} \qquad 3.1.21a$$

22

Once a solution is obtained by numerical integration, it is possible to compare this more exact solution with the Langmuir-Childs solution. This is done by deriving an expression that is unity in the limit of

$$\frac{kT}{|e|} << V_A - V_C$$

This expression is:

$$\frac{9}{4} \frac{|j| x_A^2}{\varepsilon_0 (V_A - V_C) \sqrt{\frac{2|e|(V_A - V_C)}{m}}}$$

$$= \frac{9/4 \; \xi_A^2 \; M_C^{1/3}}{\left[M_A^2 - M_C^2 + 3 \{ \frac{1}{M_A^{2/3}} - \frac{1}{M_C^{2/3}} \} \right]^{3/2}}$$

$$= L - C. C.$$

An expression for the voltage can be derived in terms of the cathode temperature and the "Mach Numbers" at the cathode and anode.

$$V_A - V_C = \frac{\gamma k T_C}{2|e|} \left[\frac{2}{\gamma-1} \{ (\frac{M_C}{M_A})^{\gamma-1} -1 \} + M_C^{\gamma-1} (M_A^2 - M_C^2) \right]$$

in evaluating this expression a cathode temperature of $3000^\circ K$ was used.

$$T_C = 3000^\circ K$$

23

A reference distance can be computed by using the maximum emission capability of tungsten at 3000°K as the "Mach 1" condition to evaluate n_c.

$$n_c = \frac{|j|}{|e|\,a_c}$$

$$(x_{ref})^2 = \frac{\epsilon_o\,m\,a_c^2}{2|e|^2\,n_c}$$

where

ϵ_o = 8.85×10^{-12} Farads/meter

m = 9.11×10^{-31} Kgm

a_c = $\sqrt{\dfrac{\gamma\,k\,T_c}{m}}$

   = 2.75×10^5 m/sec

$|e|$ = 1.60×10^{-19} coulombs

$|j|$ = 1.42×10^5 amps/meter^2

then

n_c = 3.23×10^{18}/meter^3

x_{ref} = 1.92×10^{-6} meters

COMPARISON WITH LANGMUIR CALCULATIONS

When T $=$ 2400^0K

j $=$ $.16 \times 10^4$

a_c $=$ 2.46×10^5

n_c $=$ 4.07×10^{16}

x_{ref} $=$ 1.53×10^{-5} m

For x_A $=$ 5×10^{-2} meters

ξ_A $=$ 3268

Note: $\dfrac{\gamma}{\gamma-1} \dfrac{k\,T_c}{|e|} = \dfrac{2.5 \times 1.38 \times 10^{-23} \times 2400}{1.6 \times 10^{-19}}$

$= .518$

COMPARISON WITH LANGMUIR CALCULATIONS (continued)

I/I_o	$V_A - V_c$		V_m		x_m(cm)		L-C.C.	
	Lang-muir	This Study	Lang-muir	This Study	Lang-muir	This Study	Lang-muir	This Study
.001	2.5	29.2	-1.45	-.511	.074	.0291	4.22	1.078
.01	24.4	231	-.95	-.485	.0224	.0161	1.424	1.037
.1	131.6	1760	-.48	-.369	.0062	.0070	1.134	1.012
1.0	645	14400	0	0	0	0	1.045	1.015

26

3.2   Phase II

No Collisions between Ions and Electrons
One-dimensional flow.

Electrons

Mass

$$j_e = - |e| \, n_e \, u_e \qquad\qquad 3.2.1$$

Momentum

$$m_e \, n_e \, u_e \frac{\partial u_e}{\partial x} + \frac{\partial p_e}{\partial x} = - |e| \, n_e \, E \qquad\qquad 3.2.2$$

Energy

$$n_e \, u_e \frac{\partial}{\partial x} \left(\frac{5}{2} \, kT_e + m_e \frac{u_e^2}{2} \right) = - |e| \, n_e \, u_e \, E \qquad 3.2.3$$

Entropy

$$\left(\frac{(kT_e)}{kT_e^{**}} \right)^{5/2} = \left(\frac{p_e}{p_e^{**}} \right) ;$$

$$\left(\frac{(kT_e)}{kT_e^{**}} \right)^{3/2} = \left(\frac{n_e}{n_e^{**}} \right) = \frac{u_e^{**}}{u_e} \qquad\qquad 3.2.4$$

Ions

Mass

$$j_i = Z \, |e| \, n_i \, E \qquad\qquad 3.2.5$$

Momentum

$$m_i \, n_i \, u_i \frac{\partial u_i}{\partial x} + \frac{\partial p_i}{\partial x} = Z \, |e| \, n_i \, E \qquad\qquad 3.2.6$$

3.2 Phase II

No Collisions between Ions and Electrons
One-dimensional flow.

Electrons

Mass
$$j_e = - |e| \, n_e \, u_e \qquad\qquad 3.2.1$$

Momentum
$$m_e \, n_e \, u_e \frac{\partial u_e}{\partial x} + \frac{\partial p_e}{\partial x} = - |e| \, n_e \, E \qquad\qquad 3.2.2$$

Energy
$$n_e \, u_e \frac{\partial}{\partial x} \left(\frac{5}{2} \, kT_e + m_e \frac{u_e^2}{2} \right) = - |e| \, n_e \, u_e \, E \qquad 3.2.3$$

Entropy
$$\left(\frac{(kT_e)}{kT_e^{**}} \right)^{5/2} = \left(\frac{p_e}{p_e^{**}} \right) \, ;$$

$$\left(\frac{(kT_e)}{kT_e^{**}} \right)^{3/2} = \left(\frac{n_e}{n_e^{**}} \right) = \frac{u_e^{**}}{u_e} \qquad\qquad 3.2.4$$

Ions

Mass
$$j_i = Z \, |e| \, n_i \, E \qquad\qquad 3.2.5$$

Momentum
$$m_i \, n_i \, u_i \frac{\partial u_i}{\partial x} + \frac{\partial p_i}{\partial x} = Z \, |e| \, n_i \, E \qquad\qquad 3.2.6$$

29

Energy

$$n_i \, u_i \, \frac{\partial}{\partial x} \left(\frac{5}{2} \, kT_i + m_i \, \frac{u_i^2}{2} \right) = $$

$$Z \, |e| \, n_i \, u_i \, E \qquad\qquad 3.2.7$$

Entropy

$$\left(\frac{kT_i}{kT_i^{*}} \right)^{5/2} = \frac{p_i}{p_i^{*}} \quad ;$$

$$\left(\frac{kT_i}{kT_i^{**}} \right)^{3/2} = \left(\frac{n_i}{n_i^{*}} \right) = \frac{u_i^{*}}{u_i} \qquad\qquad 3.2.8$$

Poisson "coupling" relation

$$\epsilon_o \, \frac{\partial E}{\partial x} = |e| \left(Z \, n_i - n_e \right) \qquad\qquad 3.2.9$$

Determine "Critical" Conditions

$$\frac{\partial p_e}{\partial x} = kT_e \, \frac{\partial n_e}{\partial x} + n_e \, \partial \frac{kT_e}{\partial x}$$

from 3.2.1 $\quad \dfrac{1}{n_e} \, \dfrac{\partial n_e}{\partial x} = \dfrac{1}{u_e} \, \dfrac{\partial u_e}{\partial x}$

from 3.2.3 $\quad n_e \, \dfrac{\partial kT_e}{\partial x} = - \dfrac{2}{5} \, |e| \, n_e \, E \, \dfrac{2}{5} \, m_e \, u_e \, n_e \, \dfrac{\partial u_e}{\partial x}$

30

Substitute in 3.2.2

$$n_e \left(\frac{3}{5} \ m_e \ u_e - \frac{kT_e}{u_e} \right) \frac{\partial u_e}{\partial x} = - \frac{3}{5} \ |e| \ n_e \ E$$

$$\left(u_e - \frac{5}{3} \frac{kT_e}{m_e \ u_e} \right) \frac{\partial u_e}{\partial x} = - \frac{|e|}{m_e} \ E \qquad\qquad 3.2.10$$

Critical condition

$$\left(u_e** \right)^2 = \frac{5}{3} \frac{kT_e**}{m_e} \qquad\qquad E** = 0$$

Using 3.2.4 $\qquad kT_e = kT_e** \left(\frac{u_e**}{u_e} \right)^{2/3}$

$$\therefore \left\{ \frac{u_e}{u_e**} - \frac{5}{3} \frac{kT_e**}{m_e \ u_e**^2} \left(\frac{u_e**}{\bar{u}_e} \right)^{5/3} \right\} \frac{\partial}{\partial x} \left(\frac{u_e}{u_e**} \right) = - \frac{|e| \ E}{m_e \ u_e**^2}$$

$$\text{or} \qquad \left(U_e - \frac{1}{U_e{}^{5/3}} \right) \frac{\partial U_e}{\partial \eta} = \frac{|e|}{m_e \ u_e**^2} \frac{\partial \Phi}{\partial \eta} \qquad\qquad 3.2.10a$$

$$\frac{U_e{}^2}{2} + \frac{3}{2} \frac{1}{U_e{}^{2/3}} - \left(\frac{1}{2} + \frac{3}{2} \right) = \frac{|e| \ \Phi}{m_e \ u_e**^2}$$

31

$$\frac{U_e^2}{2} + \frac{3}{2} \frac{1}{U_e^{2/3}} = 2 + \frac{|e| \phi}{m_e u_e^{**2}}$$

3.2.11

Similarly for the ions

$$(u_i^*)^2 = \frac{5}{3} \frac{kT_i^*}{m_i} \qquad E^* = 0$$

3.2.12

$$\frac{U_i^2}{2} + \frac{3}{2} \frac{1}{U_i^{2/3}} = 2 + \frac{Z |e| (\phi^* - \phi)}{m_i u_i^{*2}}$$

3.2.13

The two momentum equations, 3.2.2 and 3.2.5 can be added together and integrated to give:

$$p_i \left(1 + \frac{m_i u_i^2}{kT_i} \right) + p_e \left(1 + \frac{m_e u_e^2}{kT_e} \right) + \frac{\varepsilon_o E^2}{2} =$$

$$p_i^* \left(1 + \frac{m_i u_i^{*2}}{kT_i^*} \right) + p_e^* \left(1 + \frac{m_e u_e^{*2}}{kT_e^*} \right) =$$

$$p_i^{**} \left(1 + \frac{m_i u_i^{**2}}{kT_i^{**}} \right) + p_e^{**} \left(1 + \frac{m_e u_e^{**2}}{kT_e^{**}} \right)$$

3.2.14

32

Using the sonic conditions

$$\frac{8}{5} \; p_i{}^* + \left(1 + \frac{5}{3} \; \frac{T_e{}^{**}}{T_e{}^*} \; U_e{}^{*2}\right) p_e{}^* \; =$$

$$\left(1 + \frac{5}{3} \; \frac{T_i{}^*}{T_i{}^{**}} \; U_i{}^{**2}\right) p_e{}^{**} \; + \; \frac{8}{5} \; p_e{}^{**} \qquad\qquad 3.2.1.4a$$

Also

$$p_i{}^{**} \; = \; p_i{}^* \; \frac{1}{U_i{}^{**5/3}} \qquad\qquad p_e{}^* \; = \; p_e{}^{**} \frac{1}{U_e{}^{*5/3}}$$

and $\quad T_i{}^{**} \; = \; T_i{}^*/U_i{}^{**2/3}, \quad T_i{}^* \; = \; T_i{}^{**}/U_e{}^{*2/3}$

$$\therefore \qquad p_i{}^* \left(\frac{8}{5} \; - \; \frac{1}{U_i{}^{**5/3}} \; - \; \frac{5}{3} \; U_i{}^{**} \quad\right) \; =$$

$$p_e{}^{**} \left(\frac{8}{5} \; - \; \frac{1}{U_e{}^{*5/3}} \; - \; \frac{5}{3} \; U_e{}^* \quad\right) \qquad\qquad 3.2.14b$$

Using equations 3.2.11 and 3.2.13

$$m_e \; u_e{}^{**2} \; \left\{\frac{U_e{}^{*2}}{2} \; + \; \frac{3}{2 \; U_e{}^{*2/3}} \; - \; 2\right\} \; =$$

$$\frac{m_i \; u_i{}^*}{Z} \; \left\{\frac{U_i{}^{**2}}{2} \; + \; \frac{3}{2 \; U_i{}^{**2/3}} \; - \; 2\right\} \qquad\qquad 3.2.15$$

33

or

$$kT_e** \{ \frac{U_e*^2}{2} + \frac{3}{2 \, U_e*^{2/3}} - 2 \} =$$

$$\frac{kT_i*}{Z} \{ \frac{U_i**^2}{2} + \frac{3}{2 \, U_i**^{2/3}} - 2 \} \qquad 3.2.15a$$

Equations 3.2.14b and 3.2.15a permit us to evaluate the
"terminal velocities U_i** and U_e* in terms of the ratios of
the electron and ion pressures and temperatures at the two
"critical" positions.

3.3 Phase III

Plasma and Current Flow
No Collision Interaction

Electrons

Mass Flow

$$m_e \, n_e \, u_e \, A = \dot{m}_e \qquad \qquad 3.3.1$$

Momentum

$$m_e \, n_e \, u_e \, \frac{\partial u_e}{\partial x} + \frac{\partial p_e}{\partial x} = - |e| \, n_e \, E - m_e \, n_e F_g \quad 3.3.2$$

Energy

$$n_e \, u_e \, \frac{\partial}{\partial x} \left(\frac{5}{2} \, kT_e + m_e \, \frac{u_e^2}{2} \right) =$$

$$- |e| \, n_e \, u_e \, E - n_e \, n_e \, u_e \, F_g \qquad \qquad 3.3.3$$

Entropy

$$\left(\frac{kT_e}{kT_e^*} \right)^{5/2} = \frac{p_e}{p_e^*} \qquad \qquad 3.3.4$$

Ions

Mass Flow

$$m_i \, n_i \, u_i \, A = \dot{m}_i \qquad \qquad 3.3.5$$

Momentum

$$m_i \, n_i \, u_i \, \frac{\partial u_i}{\partial x} + \frac{\partial p_i}{\partial x} =$$

$$|e| \, Z \, n_i \, E - m_i \, n_i \, F_g \qquad \qquad 3.3.6$$

Energy
$$n_i \, u_i \, \frac{\partial}{\partial x} \left(\frac{5}{2} \, kT_i \, + \, m_i \, \frac{u_i^2}{2} \right) \, =$$

$$|e| \, Z \, n_i \, u_i \, E \, - \, m_i \, n_i \, u_i \, F_g \qquad\qquad 3.3.7$$

Entropy
$$\left(\frac{kT_i}{kT_i^*} \right)^{5/2} = \; \frac{p_i}{p_i^*} \qquad\qquad 3.3.8$$

Poisson's Equation

$$\frac{\varepsilon_o}{A} \; \frac{\partial EA}{\partial x} \; = \; |e| \, (Z \, n_i \, - \, n_e) \qquad\qquad 3.3.9$$

Current Density

$$j \, = \, \frac{Z|e|}{m_i} \; \frac{\dot{m}_i}{A} \; - \; \frac{|e|}{m_e} \; \frac{\dot{m}_e}{A}$$

Derive critical condition for ions

$$\frac{\partial p_i}{\partial x} \; = \; n_i \, \frac{\partial kT_i}{\partial x} \; + \; kT_i \, \frac{\partial n_i}{\partial x}$$

from continuity

$$\frac{\partial n_i}{\partial x} = -n_i \left(\frac{1}{u_i} \frac{\partial u_i}{\partial x} + \frac{1}{A} \frac{\partial A}{\partial x} \right)$$

from energy

$$n_i \frac{\partial k T_i}{\partial x} = -\frac{2}{5} m_i n_i u_i \frac{\partial u_i}{\partial x} +$$

$$\frac{2}{5} Z |e| n_i E - \frac{2}{5} m_i n_i F_g$$

Momentum equation becomes

$$\left\{ \left(1 + \frac{2}{5}\right) u_i - \frac{k T_i}{m_i u_i} \right\} \frac{\partial u_i}{\partial x} =$$

$$\left(1 - \frac{2}{5}\right) \frac{Z |e| E}{m_i} - \left(1 - \frac{2}{5}\right) F_g + \frac{k T_i}{m_i A} \frac{\partial A}{\partial x}$$

or

$$\left(u_i - \frac{5}{3} \frac{k T_i}{m_i u_i} \right) \frac{\partial u_i}{\partial x} =$$

$$\frac{Z |e| E}{m_i} - F_g + \frac{5}{3} \frac{k T_i}{m_i A} \frac{\partial A}{\partial x} \qquad 3.3.10$$

To eliminate the ion temperature, use entropy condition that

$$\left(\frac{kT_i}{kT_i^*}\right)^{3/2} = \left(\frac{n_i}{n_i^*}\right) = \frac{A^* \, u_i^*}{A \, u_i}$$

and put $\quad u_i = u_i^* \, U_i .$

$$\left\{ U_i - \left(\frac{A^*}{A}\right)^{2/3} \frac{1}{U_i^{5/3}} \right\} \frac{\partial U_i}{\partial x} \quad =$$

$$\frac{Z \, |e| \, E}{m_i \, u_i^{*2}} \; - \; \frac{F_g}{u_i^{*2}} \; + \; \frac{1}{U_i^{2/3}} \left(\frac{A^*}{A}\right)^{5/3} \frac{\partial}{\partial x} \left(\frac{A}{A^*}\right) \qquad 3.3.11$$

Next, eliminate E by multiplying 3.3.11 and A/A^* and differentiating. First, define

$$\frac{A}{A^*} = \eta$$

Considering the left hand side first

$$\frac{\partial}{\partial \chi} \left\{ \left(\eta \, U_i - \frac{\eta^{1/3}}{U_i^{5/3}} \right) \frac{\partial_i}{\partial x} \right\} \quad =$$

$$\left(\eta \, U_i - \frac{\eta^{1/3}}{U_i^{5/3}} \right) \frac{\partial^2 \, U_i}{\partial \, x^2} + \left(\eta + \frac{5}{3} \, \frac{\eta^{1/3}}{U_i^{8/3}} \right) \left(\frac{\partial U_i}{\partial x} \right)^2 +$$

$$\left(U_i - \frac{1}{3} \, \frac{1}{\eta^{2/3} \, U_i^{5/3}} \right) \, \frac{\partial U_i}{\partial x} \quad \frac{\partial \eta}{\partial x}$$

Consider next the right hand side

$$\frac{\partial}{\partial x} \left\{ \frac{Z \, |e| \, \eta \, E}{m_i \, u_i^{*2}} - \eta \, \frac{F_i}{u_i^{*2}} + \frac{1}{U_i^{2/3} \, \eta^{2/3}} \, \frac{\partial \eta}{\partial x} \right\} =$$

$$\frac{Z \, |e|}{m_i \, u_i^{*2}} \, \frac{\partial \eta E}{\partial x} - \frac{\eta}{u_i^{*2}} \, \frac{\partial F_g}{\partial x} - \frac{F_g}{u_i^{*2}} \, \frac{\partial \eta}{\partial x} -$$

$$\frac{2}{3} \left\{ \frac{1}{U_i^{5/3} \, \eta^{2/3}} \, \frac{\partial U_i}{\partial x} + \frac{1}{U_i^{2/3} \, \eta^{5/3}} \, \frac{\partial \eta}{\partial x} \right\} \frac{\partial \eta}{\partial x} +$$

$$\frac{1}{U_i^{2/3} \, \eta^{2/3}} \, \frac{\partial^2 \eta}{\partial x^2}$$

Collecting terms and using equation 3.3.9, we obtain a second order differential equation for the ion velocity

$$\left(\eta U_i - \frac{\eta^{1/3}}{U_i^{5/3}} \right) \frac{\partial^2 U_i}{\partial x^2} + \left(\eta + \frac{5}{3} \frac{1/3}{U_i^{8/3}} \right) \left(\frac{\partial U_i}{\partial x} \right)^2 +$$

$$\left(U_i + \frac{1}{3} \frac{1}{\eta^{2/3} U_i^{5/3}} \right) \frac{\partial U_i}{\partial x} \frac{\partial \eta}{\partial x} =$$

$$\frac{z^2 |e|^2 \dot{m}_i}{\epsilon_o m_i^2 u_i^{*3} A^* U_i} \left(1 - \frac{\dot{m}_e}{z \dot{m}_i} \frac{m_i u_i}{m_e u_e} \right) -$$

$$\frac{\eta}{u_i^{*2}} \frac{\partial F_g}{\partial x} - \frac{F_g}{u_i^{*2}} \frac{\partial \eta}{\partial x} - \frac{2}{3} \frac{1}{U_i^{2/3} \eta^{5/3}} \left(\frac{\partial \eta}{\partial x} \right)^2 +$$

$$\frac{1}{U_i^{2/3} \eta^{2/3}} \frac{\partial^2 \eta}{\partial x^2} \qquad\qquad 3.3.12$$

Equation 3.3.12 couples the ion and electron velocities. Therefore, a differential equation for the electron velocity must next be derived. Proceeding as above for the ions, the electron momentum equation becomes

$$\left(u_e - \frac{5}{3} \frac{kT_e}{m_e u_e} \right) \frac{\partial u_e}{\partial x} = -\frac{|e| E}{m_e} - F_g + \frac{5}{3} \frac{kT_e}{m_e A} \frac{\partial A}{\partial x}$$

The electron temperature can now be eliminated by
introducing the entropy constraint for the electrons, namely

$$\frac{kT_e}{kT_e{}^*} = \left(\frac{A^*\ u_e{}^*}{A\ u_e}\right)^{2/3}$$

also let

$$\frac{u_e}{u_i{}^*} = U_e \qquad \text{and} \qquad \frac{T_e{}^*}{T_i{}^*} = \tau^*$$

then

$$\left(U_e - \tau^*\ \frac{m_i}{m_e}\ \frac{U_e{}^{*2/3}}{\eta^{2/3}\ U_e{}^{5/3}}\right)\ \frac{\partial U_e}{\partial x} =$$

$$-\ \frac{|e|\ E}{m_e\ u_i{}^{*2}}\ -\ \frac{F_g}{u_i{}^{*2}}\ +\ \tau^*\ \frac{m_i}{m_e}\ \frac{U_e{}^{*2/3}}{\eta^{5/3}\ U_e{}^{2/3}}\ \frac{\partial\eta}{\partial x} \qquad 3.3.13$$

The electric field can be eliminated from this equation in the
same manner as it was in the equation for the ion velocity.
The result is a second order differential equation for the
electron velocity. For convenience, define

$$\frac{m_i}{m_e}\ \tau^*\ U_e{}^{*2/3} = X \qquad 3.3.14$$

41

$$\frac{Z \, |e|^2 \, x^{*2}}{m_i \, u_i^{*3} \, A^* \, \varepsilon_o} \left(\frac{Z \dot{m}_i}{m_i} + \frac{I}{|e|} \right) = Y \qquad\qquad 3.3.15$$

The differential equation for the electron velocity becomes

$$\left(\eta \, U_e - \frac{X \eta^{1/3}}{U_e^{5/3}} \right) \frac{\partial^2 U_e}{\partial x^2} + \left(\eta + \frac{5}{3} \frac{X \, \eta^{1/3}}{U_e^{8/3}} \right) \left(\frac{\partial U_e}{\partial x} \right)^2 +$$

$$\left(U_e + \frac{X}{3 \eta^{2/3} \, U_e^{5/3}} \right) \frac{\partial U_e}{\partial x} \frac{\partial \eta}{\partial x} =$$

$$- \frac{\eta}{u_i^{*2}} \frac{\partial F_g}{\partial x} - \frac{F_g}{u_i^{*2}} \frac{\partial \eta}{\partial x} - \frac{2}{3} \frac{X}{U_e^{2/3} \, \eta^{5/3}} \left(\frac{\partial \eta}{\partial x} \right)^2 +$$

$$\frac{X}{U_e^{2/3} \, \eta^{2/3}} \frac{\partial^2 \eta}{\partial x^2} \qquad\qquad 3.3.16$$

$$- \frac{Y}{Z \, x^{*2}} \frac{m_i}{m_e} \left\{ \frac{1}{1+\mathcal{A}} \left(\frac{1}{U_i} \frac{1}{U_e} \right) + \frac{\mathcal{A}}{1+\mathcal{A}} \frac{1}{U_e} \right\}$$

where

$$\mathcal{A} = \frac{m_i \, I}{Z \, |e| \, \dot{m}_i} \qquad\qquad 3.3.17$$

42

In some cases, it is more convenient to use a relation between the ion and electron velocities

$$\left(Z \frac{m_e}{m_i} U_e - \frac{\tau^* Z U_e^{*2/3}}{\eta^{2/3} U_e^{5/3}} \right) \frac{\partial U_e}{\partial x} + \left(U_i - \frac{1}{\eta^{2/3} U_i^{5/3}} \right) \frac{\partial U_i}{\partial x} =$$

$$- \left(1 + Z \frac{m_e}{m_i} \right) \frac{F_g}{u_i^{*2}} + \frac{1}{\eta^{5/3}} \left(\frac{1}{U_i 2/3} + \frac{Z \tau^* U_e^{*2/3}}{U_e^{2/3}} \right) \frac{\partial \eta}{\partial x} \qquad 3.3.18$$

The above equations, together with the appropriate boundary conditions permit solutions to a wide variety of problems.

Boundary Conditions

Some boundary conditions are obtained at the position where the ion velocity is critical. These are listed below

$$U_i^{*2} = \frac{m_i u_i^{*2}}{\frac{5}{3} kT_i^*} = 1$$

$$\frac{Z |e| E^*}{m_i u_i^{*2}} = \frac{F_g^*}{u_i^{*2}} - \left(\frac{\partial \eta}{\partial x} \right)^*$$

43

$$\frac{8}{3} \left\{ \left(\frac{\partial U_i}{\partial x} \right)^* \right\}^2 + \frac{4}{3} \left(\frac{\partial U_i}{\partial x} \right)^* \left(\frac{\partial \eta}{\partial x} \right)^* =$$

$$\frac{Y}{(x^*)^2} \left\{ \frac{1}{1+\delta} \left(1 - \frac{1}{U_e^*} \right) + \frac{\delta}{(1+\delta) \, U_e^*} \right\}$$

$$- \frac{1}{u_i^{*2}} \left\{ \left(\frac{\partial F_g}{\partial x} \right)^* - F_g^* \left(\frac{\partial \eta}{\partial x} \right)^* \right\} - \frac{2}{3} \left\{ \left(\frac{\partial \eta}{\partial x} \right)^* \right\}^2 + \left(\frac{\partial^2 \eta}{\partial x^2} \right)^*$$

$$\left(Z \frac{m_e}{m_i} \, U_e^* - \frac{Z \tau^*}{U_e^*} \right) \left(\frac{\partial U_e}{\partial x} \right)^* =$$

$$- \left(1 + Z \frac{m_e}{m_i} \right) \frac{F_g^*}{u_i^{*2}} + \left(1 + Z \tau^* \right) \left(\frac{\partial \eta}{\partial x} \right)^*$$

A similar set of boundary conditions are obtained where the electron velocity becomes critical, these are listed below

$$\left(U_e^{**} \right)^2 = \frac{m_i}{m_e} \frac{\tau^*}{(\eta^{**})^{2/3}} \left(\frac{U_e^*}{U_e^{**}} \right)^{2/3}$$

$$\frac{|e| \, E^{**}}{m_e \, u_i^{*2}} = - \frac{F_g^{**}}{u_i^{*2}} + \frac{(U_e^{**})^2}{\eta^{**}} \left(\frac{\partial \eta}{\partial x}\right)^{**}$$

since

$$\left(U_e^{**}\right)^{8/3} = \frac{X}{(\eta^{**})^{2/3}}$$

$$\frac{8}{3} \, \eta^{**} \left\{ \left(\frac{\partial U_e}{\partial x}\right)^{**} \right\}^2 + \frac{4}{3} \, U_e^{**} \left(\frac{\partial U_e}{\partial x}\right)^{**} \left(\frac{\partial \eta}{\partial x}\right)^{**} =$$

$$- \frac{Y}{Zx^{*2}} \, \frac{m_i}{m_e} \left\{ \frac{1}{1+\mathcal{J}} \left(\frac{1}{U_i^{**}} - \frac{1}{U_e^{**}}\right) + \frac{\mathcal{J}}{1+\mathcal{J}} \, \frac{1}{U_{e*}} \right\}$$

$$- \frac{\eta^{**}}{u_i^{*2}} \left(\frac{\partial F_g}{\partial x}\right)^{**} - \frac{F_g^{**}}{u_i^{*2}} \left(\frac{\partial \eta}{\partial x}\right)^{**} -$$

$$\frac{2}{3} \, \frac{(U_e^{**})^2}{\eta^{**}} \left\{ \left(\frac{\partial \eta}{\partial x}\right)^{**} \right\}^2 + \left(U_e^{**}\right)^2 \left(\frac{\partial^2 \eta}{\partial x^2}\right)^{**}$$

$$\left\{ U_i{}^{**} - \frac{1}{(\eta{}^{**})^{2/3} (U_i{}^{**})^{5/3}} \right\} \left(\frac{\partial U_i}{\partial x} \right)^{**} =$$

$$- \left(1 + \frac{Z \, m_e}{m_i} \right) \frac{F_g{}^{**}}{u_i{}^{*2}} + \frac{1}{(\eta{}^{**})^{5/3}} \quad x$$

$$\left\{ \frac{1}{U_i{}^{**2/3}} + \frac{Z \, \tau^* \, U_e{}^{*2/3}}{(U_e{}^{**})^{2/3}} \right\} \left(\frac{\partial \eta}{\partial x} \right)^*$$

3.4   Procedure to Evaluate Solution for
       Counter-flowing Ions and Electrons.

1)   Choose values for the following quantities

   i)   The non-dimensional potential drop

$$\phi^* = \frac{|e|\,\phi^*}{m_e\,u_e^{**2}} = \frac{|e|\,\phi^*}{\frac{5}{3}\,kT_e^{**}}$$ 3.4.1

   ii) The charge on the ion, Z.

   iii) The ratio of the critical values of the
        electron to ion temperature,

$$\frac{T_e^{**}}{T_i^*} = \tau$$ 3.4.2

2)   Using the electron energy equation, by iteration,
       evaluate the non-dimensional electron velocity at
       the position where the ion velocity is critical.

$$\left(u_e^*\right)_{j+1} = \left\{ 4 + 2\,\phi^* - \frac{3}{u_{e\,j}^{*\,2/3}} \right\}^{1/2}$$ 3.4.3

47

3) Using the ion energy equation, by iteration, evaluate the non-dimensional ion velocity at the position where the electron velocity is critical.

$$\left(U_i^{**}\right)_{j+1} = \left\{4 + 2\,\frac{ZT_e^{**}}{T^*}\,\phi^* - \frac{3}{\left(U_i^{**}\right)_j^{2/3}}\right\}^{1/2} \qquad 3.4.4$$

4) Make a first choice of the value of the "Childs-Langmuir", constant L.C.

$$Y_j = \frac{|e|\,|j_e|\,x^{*2}}{\varepsilon_o\,m_e\,u_e^{**3}\,\phi^*\,U_e^*} = L.C._j\,\left[\frac{2\phi^*}{U_e^*}\right]^{1/2} \qquad 3.4.5$$

5) Evaluate the ratio of the values of the ion pressure and electron pressure at their respective critical positions

$$\frac{P_i^*}{P_i^{**}} = \frac{\dfrac{8}{5} - \dfrac{1}{U_e^{*\,5/3}} - \dfrac{5}{3}U_e^*}{\dfrac{8}{5} - \dfrac{1}{U_i^{**\,5/3}} - \dfrac{5}{3}U_i^{**}} \qquad 3.4.6$$

6)   Evaluate the charge density ratio

$$\frac{Z \, n_i^*}{n_e^{**}} = \frac{P_i^*}{P_i^{**}} \quad \frac{Z \, kT_e^{**}}{kT_i^*} \qquad\qquad 3.4.7$$

7)   Numerically integrate Poisson's Equation,

$$\frac{d^2}{d_\eta^{\,2}} \left(\frac{\phi}{\phi^*} \right) = Y \left(\frac{U_e^*}{U_e} - \frac{Zn_i^*}{n_e^{**}} \, \frac{U_e^*}{U_i} \right) \qquad\qquad 3.4.8$$

Using the energy rela ions as follows:

a)   when $0 > \eta < |$; $U_e + U_i > 1.$

iterate for U_e and U_i using equations.

$$\left(U_e \right)_{j+1} = \left\{ 4 + 2\phi - \frac{3}{\left(U_e \right)_j^{2/3}} \right\}^{1/2} \qquad\qquad 3.4.9$$

$$\left[U_i\right]_{j+1} = \left\{ 4 + 2\left(\Phi^* - \Phi\right) - \frac{3}{\left[U_i\right]_j^{2/3}} \right\}^{1/2} \qquad 3.4.10$$

b) when $\eta < 0$ $U_i > 1$; $U_e < 1$.

iterate for U_i using Equation 3.4.10.

iterate for U_e using

$$\left[U_e\right]_{j+1} = \left\{ \frac{3}{4 + 2\Phi - \left[U_e\right]_j^2} \right\}^{3/2} \qquad 3.4.11$$

c) when $\eta > 1$, $U_i < 1$; $U_e > 1$.

iterate for U_e using Equation 3.4.9.

iterate for U_i using

$$\left[U_i\right]_{j+1} = \left\{ \frac{3}{4 + 2\left(\Phi^* - \Phi\right) - \left[U_i\right]_j^2} \right\}^{3/2} \qquad 3.4.12$$

50

8) Compare electric field from integration with value calculated from the momentum equation.

$$\frac{d}{d\eta}\left(\frac{\Phi}{\Phi*}\right) = Y \quad \frac{6}{5} \quad \frac{U_e*}{\Phi*} \quad \left| \frac{p_i*}{p_i**} \quad \left\{ \frac{1}{U_i^{5/3}} + \frac{5}{3} U_i - \frac{8}{3} \right\} \right.$$

$$+ \frac{1}{U_e^{5/3}} + \frac{5}{3} U_e - \frac{1}{U_e*^{5/3}} - \frac{5}{3} U_e* \left|^{1/2} \right. \qquad 3.4.13$$

9) Adjust the value of Y_j until

$$\Phi = \Phi* \qquad \text{at } \eta = 1$$

$$U_e = U_e*$$

$$U_i = 1$$

and $\qquad \dfrac{d\Phi}{d\eta} = 0$

3.5 Relations Between Actual and Non-Dimensional Variables

Inter Critical Zone Potential Drop

$$\phi = \frac{5}{3} \frac{kT_e^{**}}{|e|} \Phi^* \quad \text{volts}$$

Electric Field Strength

$$E = -\frac{5}{3} \frac{kT_e^{**}}{|e|x^*} \Phi^* \frac{d}{d\eta} \left(\frac{\phi}{\Phi^*} \right) \quad \text{volts/meter.}$$

Electron Velocity

$$u_e = \left(\frac{5}{3} \frac{kT_e^{**}}{m_e} \right)^{1/2} U_e \quad \text{m/sec.}$$

Ion Velocity

$$u_i = \left(\frac{5}{3} \frac{kT_i^*}{m_i} \right)^{1/2} U_i \quad \text{m/sec.}$$

Electron Current Density

$$|j_e| = <L.C.> \left(\frac{2|e|}{m_e}\right)^{1/2} \frac{\epsilon_o \phi *^{3/2}}{x*^2} \qquad \text{amps/m2.}$$

Ion Current Density

$$|j_i| = \left(\frac{m_e}{m_i}\right)^{1/2} |j_e| \qquad \text{amps/m}^2.$$

Some typical solutions of the equations are presented in Figures 13 through 21. A graph of the "Childs-Langmuir" coefficient as a function of the potential difference between the two critical positions is presented in Figure 22. There are a number of interesting aspects to the solutions:

1) Attempts to obtain non-symmetrical solutions have been unsuccessful. If, indeed, only symmetrical solutions exist, then the critical points will be located where

$$Z \, kT_e{}^{**} = \, kT_i{}^* \quad \text{and the following relations hold}$$

$$U_e{}^{**} = U_i{}^*$$

$$\frac{u_e{}^{**}}{u_i{}^*} = \sqrt{\frac{m_i}{Z \, m_e}}$$

$$\frac{p_e{}^{**}}{p_i{}^*} = \, 1.$$

$$\left| j_i / j_e \right| = \sqrt{\frac{Z \, m_e}{m_i}}$$

2) In the "sub-critical" region, the pressure and temperature ratios between the "critical" position and the source, usually a hot surface, can be very large.

This can be seen in Figures 15 and 18, where the logarithm of the temperature and pressure ratios are plotted as a function of the non-dimensional distance.

3)   As expected, the region of influence of the ambient or surface temperature upon the flow concentrates into smaller regions as the ratio of the potential drops to the temperature increases.

4)   Interelectrode potential drops can be much lower than the potential drop between the two critical positions.

5)   The charge neutralization that occurs due to the ion current flow permits the electron current to be up to an order of magnitude higher than occurs with space charge limited electron flow only.

4.   COMPARISON OF EXPERIMENTAL AND ANALYTIC RESULTS

The analytic results qualitatively agree with the experimental results as summarized in Fig.22 . The results cannot be expected to agree quantitively since the experiments were conducted with equipment that had cylindrical, rather than planar flow. Although the analytic procedures for calculating cylindrical counter-flow of ions and electrons are presented in this report, no solutions have been yet calculated. Another, more interesting phenomenon that has not yet been analytically treated is the development of criteria for transition from the ion-electron flow mode to the electron flow mode only. According to the experiments, this transistion occurs abruptly. It can be speculated that this occurs when the ion density at the anode drops to a value where $p_i^* < p_e^{**}$. The critical flow for the ions cannot then be established and the electric field at the anode rises abruptly.

The following description of the mechanisms in the "slow" discharge follows from the experimental and analytic studies described earlier:

1. A "discharge" that is dominated by space charge effects has been obtained. The characteristis of the discharge can be analytically investigated by study of the behaviour of counter-flowing, non-colliding electron and ion beams.

2. The discharge is initiated by application of several kilovolts between concentric electrodes, and heating the thermionic cathode, which is centrally located.

3. The space charge limited electron flow produces ions on the anode surface by inelastic collisions with the adsorbed surface layers of gas.

4. A space charge limited flow of ions towards the cathode occurs. This flow partially neutralizes the cathode space charge and permits a much higher electron

current density than occurs with electron flow only.

5. Both the electron and ion current density are controlled by a "critical flow" criterion at an electrostatic throat, rather than by emission or ion production limitations.

6. If the power density at the electrodes becomes too high, gas is desorbed at a high rate. The gas density between the electrodes can then become high enough to permit breakdown.

7. When the ion density near the anode surface drops to some critical value, the ion flow through the "electrostatic" throat cannot be established and space charge limited electron flow only, results.

8. The ratio of ion current to electron current is equal to the square root of the ratio of the electron to ion masses.

5.0   IMPLICATIONS OF THE ANALYTIC AND EXPERIMENTAL RESULTS FOR THRUSTER PERFORMANCE

Considerable insight into the performance characteristics of electromagnetic accelerators utilizing ambient gas as the propellant has been obtained from the experimental and analytic results obtained in this program. This information is summarized in the following.

5.1   MODES OF OPERATION

5.1.1   Mode I   Acceleration of Ambient Ionospheric Ions

This study could not address this mode of operation experimentally due to facility and cost limitations. Analytically, a correct solution to a properly formulated boundary value problem for this type of system is still several steps away from an orderly investigation of space charge limited flows. Further development of the approach initiated in Section 3.3 of this report should permit accurate prediction of performance potential. If this looks promising, then experiment on the space shuttle would probably be the most cost effective method of evaluating actual performance.

5.1.2   Mode II   Acceleration of Ions Produced from Adsorbed Gas Layers on or Near the Anode Surface.

The experimental and analytic investigations of this program have been primarily associated with this mode of operation, as exempified by the "slow discharge" described earlier. In terms of conventional performance parameters, this mode of operation results in very inefficient use of the electrical power. The high electron current relative to the ion current results in an "efficiency" of under 1%, where it is defined as beam power or energy divided by electrical input power or energy. The specific impulse of the exhaust beam in this mode of operation can be arbitrarily high. The ions are accelerated through most of the

58

potential drop between the electrodes, which has been experiment-
ally varied between ten thousand and several hundred volts.

5.1.3 Mode III Acceleration of Ions Produced by Volume Collisions of Gas Desorbed from Engine Structure.

This mode of operation is equivalent to that of conventional
pulsed plasma accelerators, and has been extensively studied by
many experimental and analytic groups (Refs. 25-30   ) using
injected or ablated propellant. Performance will be comparable
to that observed in such studies, and hence no detailed investiga-
tions of this mode were made.

5.1.4 Mode IV Acceleration of Ions Produced by Volume Collisional Interaction of an Extended Discharge Into the Ambient Gas.

This mode of operation had earlier been observed (Ref. 31)
in many electromagnetic accelerators with ambient pressures above
10^{-1} Torr. It was hoped that operation in this mode could be
obtained at much lower pressures by having the discharge encompass
very large volumes of gas. The tests conducted in the large tank
at General Dynamics/San Diego indicated that volume ionization
effects start to influence the discharge only a pressures of
at least 10^{-3} Torr to 10^{-4} Torr, approximately. (Initially, as
pressure is increased above these levels, phenomena occur which are
probably associated with a moving or oscillating ionization front.)
As pressures over 10^{-3} Torr occur at altitudes below 60 miles and
hence are of minimal interest for satellite propulsion,
studies were not conducted at pressures above 10^{-3} Torr, and no
further information or data generated in this study on this operating
mode.

REFERENCES

1. Demetriades, S.T., and Kretschmer, C.B., "The Use of Planetary Atmospheres for Propulsion", Armed Services Technical Info. Agency Doc. AD 154-132, (April 1958)

2. Demetriades, S.T., "A Novel System for Space Flight Using a Propulsive Fluid Accumulator", J. British Interplanetary Soc. 17, 114-119, (1959).

3. Demetriades, S.T., "Orbital Propulsion System for Space Maneuvering (PROFAC)", Astronaut, Sci. Rev. 1, 17-18 (1959).

4. Demetriades, S.T., and Young, C. F., "Orbital Refueling Satelloid", Soc. Automotive Engrs./Air Force Office Sci. Research Paper 230H (October 1960).

5. Berner, F. and Camac, M., "Air Scooping Vehicle", Avco-Everett Research Lab. Research Rept. 76, Air Force Ballistic Missile Div. TR 59-17 (August 1959)

6. Camac, M. and Berner, F., "An Orbital Air Scooping Vehicle", Astronautics 6, 28-29, 70-71, (August 1961).

7. French, E.P. "Operation of an Electric Ramjet in a Planetary Atmosphere", Am. Astronaut. Soc. Preprint, 60-90, (August 1960).

8. Glassmeyer, J.M., AFRPL "Ideagram", A-SCOR, (3 May 1970).

9. Corliss, W.R., Propulsion Systems for Space Flight, McGraw-Hill Book Co., Inc. 1968.

10. Jahn, R.G., Physics of Electric Propulsion, McGraw-Hill Book Co., Inc. 1968.

11. Ducati, A.C., et al, "Recent Progress in High Specific Impulse Thermo-Ionic Acceleration", AIAA 2nd Aerospace Sciences Meeting, New York, January 1965, (AIAA Paper 65-96).

12. Bennett, S.C. et al, "MPD Arc Jet Engine Performance", 2nd Annual Meeting, San Francisco, July 1965, (AIAA Paper 65-296).

REFERENCES (continued)

13.   Cann, G. L., et al, "Hall Current Accelerator",
        Final Report NASA Contract #NAS 3-5909.

14.   Cann, G.L. et al, "Follow-On Investigation of a
        Steady State Hall Current Accelerator", Final Report
        NASA Contract #NAS 3-3568.

15.   Moore, R. A., et al, "High Specific Impulse Thermal
        Arc Jet Thruster Technology", Technical Reports
        AFAPL-TR-65-48, Parts I and II.

16.   Cann, G. L. and Harder, R.L., "Thrust Efficiencies
        of Electromagnetic Engines", AIAA Journal, Vol. 6 No. 3,
        March 1968, pp 559-560.

17.   Cann, G. L., "The Use of E. M. Accelerators in High
        Pressure Test Facilities", ARL Report 72-0061,
        May 1972.

18.   Kogelshatz, U., "Doppler-Shift Measurements of Axial
        and Rotational Velocities in an MPD Arc", AIAA Journal,
        Vol. 8, No. 1, pp 150-154, January 1970.

19.   Mechanisms of Magnetoplasmadynamic Arc Jet
        Acceleration Processes. Contract F44620-74-C-0017,
        Interim Report #1.

20.   Mechanisms of Magnetoplasmadynamic Arc Jet Acceleration
        Processes. Contract F44620-74-C-0017-Interim
        Reports 2, 3 and 4.

21.   Langmuir, I. "The Effect of Space Charge and Residual
        Gases on Thermionic Currents in High Vacuum", Physical
        Review, Vol. II, No. 6, 450, (December 1913).

22.   Langmuir, I. "The effect of Space Charge and Initial
        Velocities on the Potential Distribution and
        Thermionic Current Between Parallel Plane Electrodes",
        Physical Review, Vol. XXI, No. 4, 419, (April 1923).

23.   Langmuir, I. "The Interaction of Electron and Positive
        Ion Space Charges in Cathode Sheaths", Physical Review,
        Vol. XXXIII, No. 6, (June 1929).

REFERENCES (continued)

24.   Collected Works of I. Langmuir.

25.   Palumbo, D.J. and Begun, M. "Plasma Acceleration in
        Pulsed Ablative Discharges", AFOSR-TR-75-0618, Air
        Force Office of Scientific Research, Bolling AFB,
        D.C., March, 1975.

26.   Palumbo, D.J. and Guman, W.J., "Effects of Electrode
        Geometry and Propellant on Pulsed Ablative Plasma
        Thruster Performance", AIAA Paper No. 75-409, March, 1975.

27.   Gooding, T.J., Hayworth, B.R., Larson, A.V., and
        Ashby, D. E. T.F., "Development of a Coaxial Plasma
        Gun for Space Propulsion", Final Report, Contract
        NAS 3-2594, NASA Report No. CR 54149, GD/Astronautics
        Report No. GDA DBA 64-051, dated June 1964.

28.   Gooding, T.J., Larson, A.V., Hayworth, B.R., and
        Ashby, D.E.T.F., "Development of a Coaxial Plasma Gun
        for Space Propulsion", Final Report, Contract NAS
        3-5759, NASA Report No. CR 54245, GD/Convair Report
        No. GDA DBA 64-052-4, dated April 1965.

29.   Gorowitz, B., Gloersen, P., and Karras, T., "Study
        of Parametric Performance of a Two-State Repetitively
        Pulsed Plasma Engine (REPPAC) Summary Report,
        NASA CR-54846, Contract No. NASw-1044, 1966.

30.   Gloersen, P., Gorowitz, B., and Kenney, J.T., "Energy
        Efficiency Trends in a Coaxial Gun Plasma Engine
        System", AIAA Journal, Vol 4, No. 3, pp 436-441,
        March 1966.

31.   Cann, G.L., et al, "Hall Current Accelerator",
        Report 5470-Final, Electro-Optical Systems, Pasadena,
        Calif. Feb 4, 1966. Also available as NASA CR 54705.
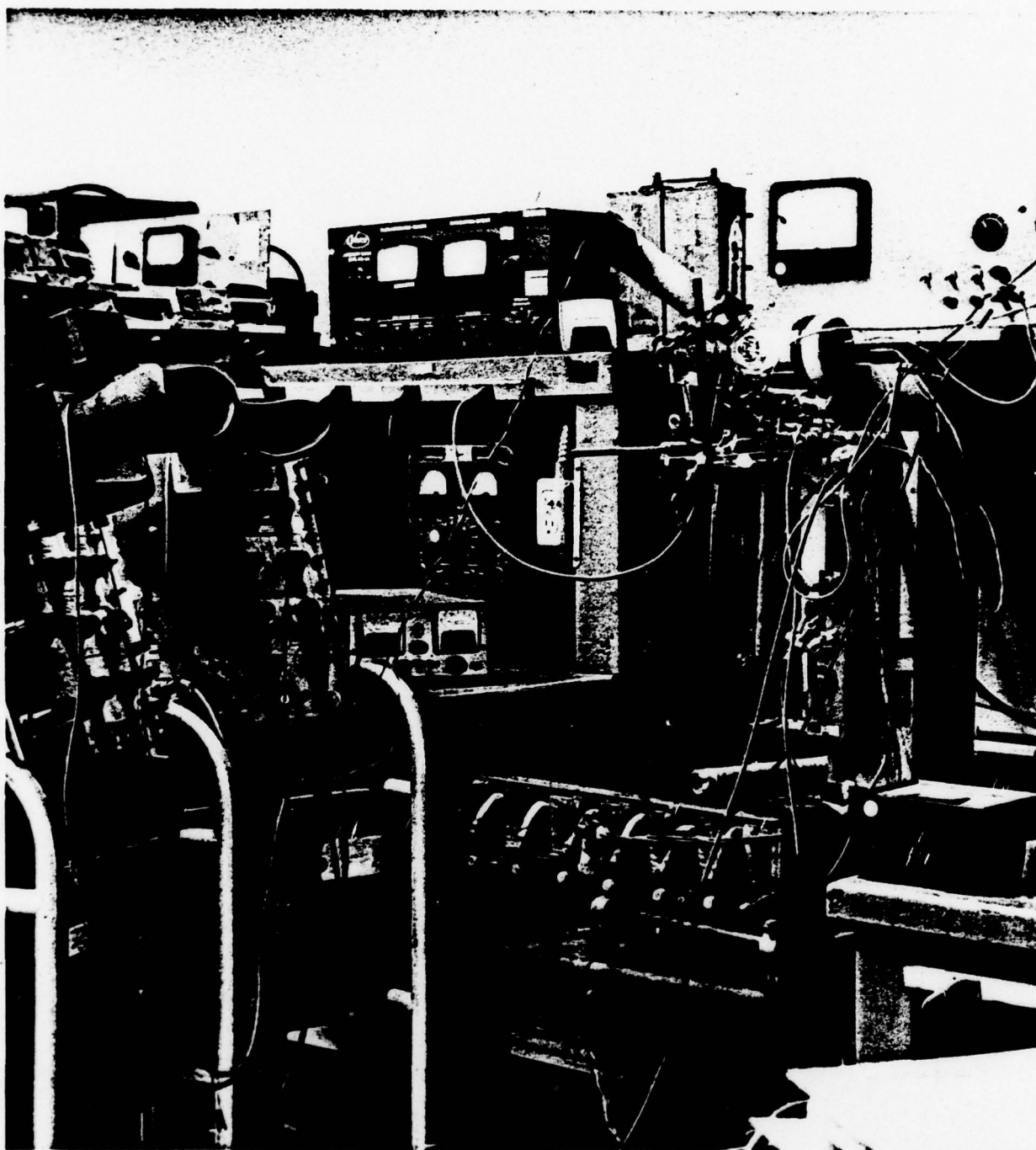
Fig. 1   Photograph of Discharge Test Cell
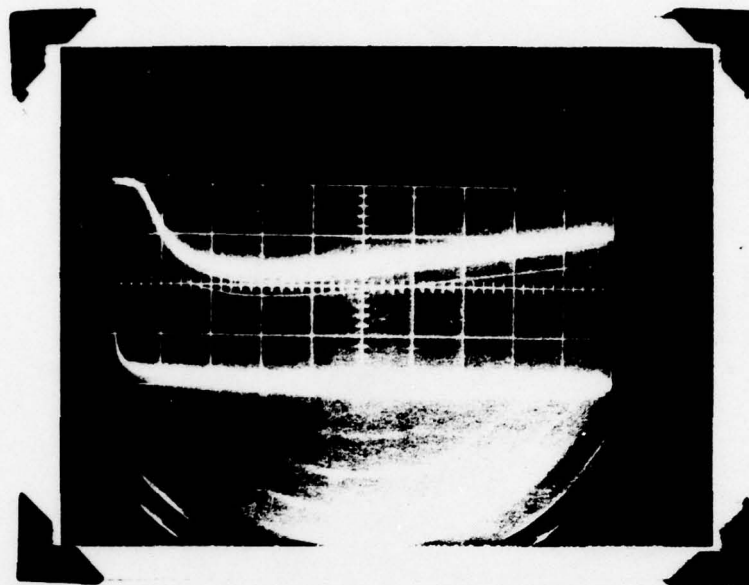
Photo-cell   .1 volts/cm

Filament current   200 amps/cm

Sweep speed   20 m. sec./cm

V = 30 volts

Fig. 2   Radiation from Filament & Current Through
the Filament.

Signal Magnet Current
Ampl/cm 20 amps
Time/cm 20 m. sec.
Magnet Vo = 50 V

Signal Filament Current
Ampl/cm 100 amps
Time/cm 20 m. sec.
Filament Vo = 30 V

Signal
Ampl/cm
Time cm

Fig. 3

Filament
and
Magnet
Currents

Signal Magnet Current
Ampl/cm 20 amps
Time/cm 20 m. sec.
Magnet Vo = 20 V

Signal Filament Current
Ampl/cm 100 amps
Time/cm 20 m. sec.
Filament Vo = 30 V

Signal Magnet Current
Ampl/cm 20 amps
Time cm 20 m. sec.

Signal Filament Current
Ampl cm 100 amps
Time/cm 20 m. sec.

Signal
Ampl cm
Time cm

65

Figure 4   Ion Detector Circuit Using NRC507 Ionization Gauge.

Signal	Voltage	p(Torr)	Signal	Current
Ampl/cm	1110 V	7 x 10⁻⁸	Ampl/cm	222 m.a.
Time/cm	10 m. sec.		Time/cm	10 m. sec.

(2)

Fig. 5   Discharge Characteristics

Signal	Voltage	p(Torr)	Signal	Current
Ampl cm	1000 V	7 x 10⁻⁷	Ampl/cm	200 m.a.
Time/cm	5 m. sec.		Time cm	5 m. sec.

(4)

Signal	Voltage	p(Torr)	Signal	Current
Ampl/cm	1110 V	3 x 10⁻⁸	Ampl/cm	222 m.a.
Time/cm	10 m. sec.		Time/cm	10 m. sec.

(1)

Signal	Voltage	p(Torr)	Signal	Current
Ampl/cm	1110 V	2.4 x 10⁻⁷	Ampl cm	222 m.a.
Time/cm	20 m. sec.		Time/cm	20 m. sec.

(3)

67

Signal   Voltage   p(Torr)Signal   Current
Amp1/cm   1000 V   3 x 10⁻⁶Amp1/cm   200 m.a.
Time/cm   5 m. sec.   Time/cm   5 m. sec.

(6)

Signal   Voltage   p(Torr)Signal   Current
Amp1 cm   1000 V   5 x 10⁻⁵Amp1/cm   200 m.a.
Time cm   5 m. sec.   Time cm   5 m. sec.

(8)

Fig. 5 . Discharge Characteristics cont'd.
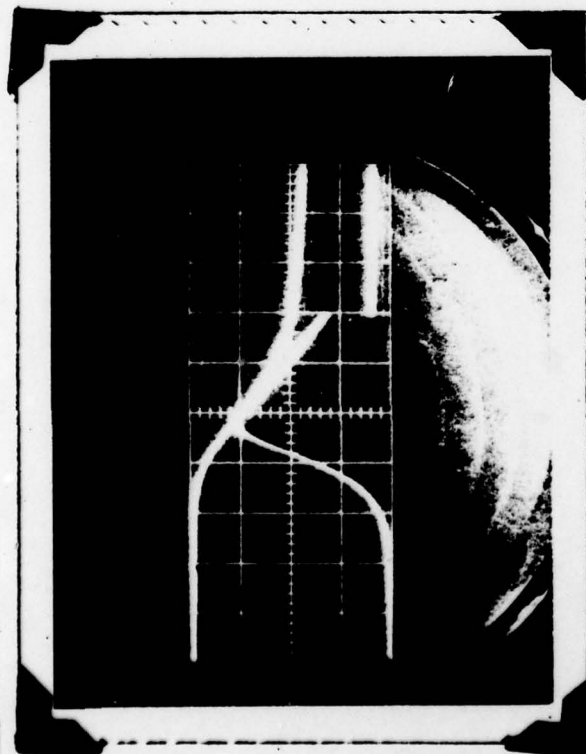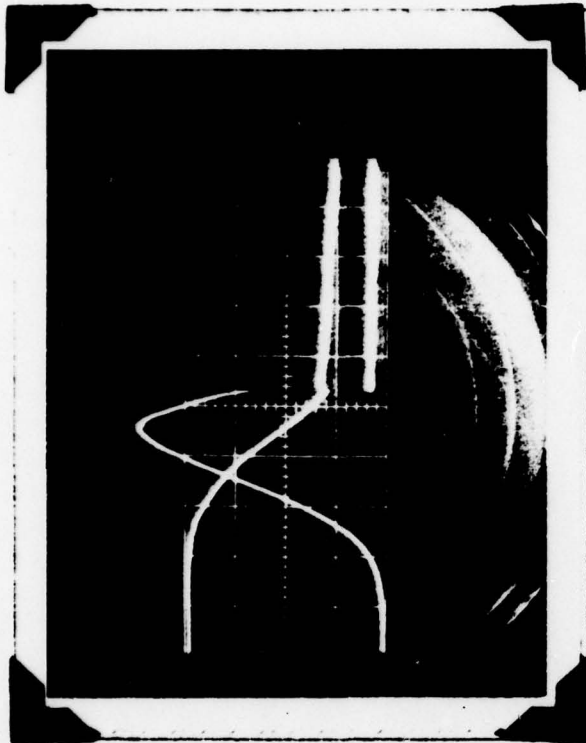
Signal   Voltage   p(Torr) Signal   Current
Amp1/cm   1000 V   1 x 10⁻⁶ Amp1/cm   200 m.a.
Time/cm   5 m. sec.   Time/cm   5 m. sec.

(5)

Signal   Voltage   p(Torr) Signal   Current
Amp1 cm   1000 V   1 x 10⁻⁵ Amp1 cm   200 m.a.
Time cm   5 m. sec.   Time/cm   5 m. sec.

(7)

68

Signal   Voltage   Signal   Current
Ampl/cm 500 V   Ampl/cm 40 m.a.
Time/cm 10 m. sec.   Time/cm 10 m. sec.
                V_o = 1500 V

(2)
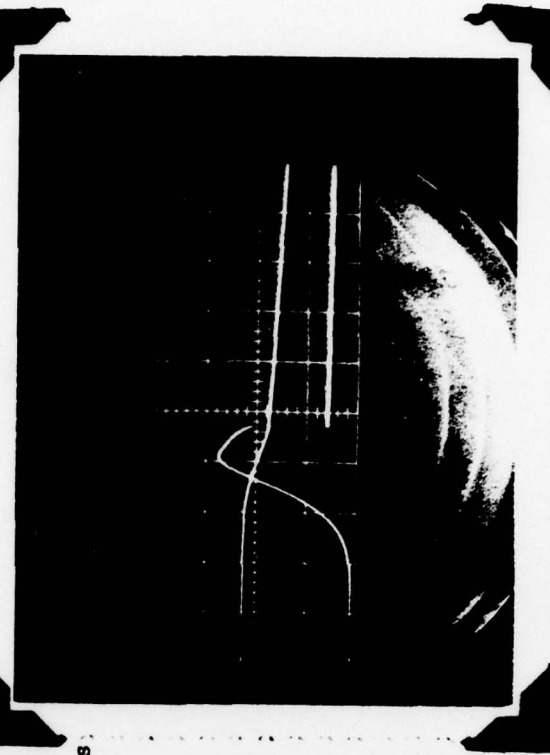
Signal   Voltage   Signal   Current
Ampl cm 1000 V   Ampl/cm 100 m.a.
Time cm 5 m. sec.   Time cm 5 m. sec.

(4)

Fig. 5a
Discharge
Characteristics
vs. Voltage on
Discharge
Condenser

Signal   Voltage   Signal   Current
Ampl/cm 500 V   Ampl/cm 20 m.a.
Time/cm 10 m. sec.   Time/cm 10 m. sec.
                V_o = 1000 V

(1)

Signal   Voltage   Signal   Current
Ampl/cm 500 V   Ampl cm 100 m.a.
Time/cm 5 m. sec.   Time/cm 5 m. sec.
                V_o = 2000 V

(3)

69

Signal __Voltage__   Signal __Current__
Ampl/cm __1000 V__   Ampl/cm __200 m. a.__
Time/cm __5 m. sec.__   Time/cm __5 m. a.__

(6)
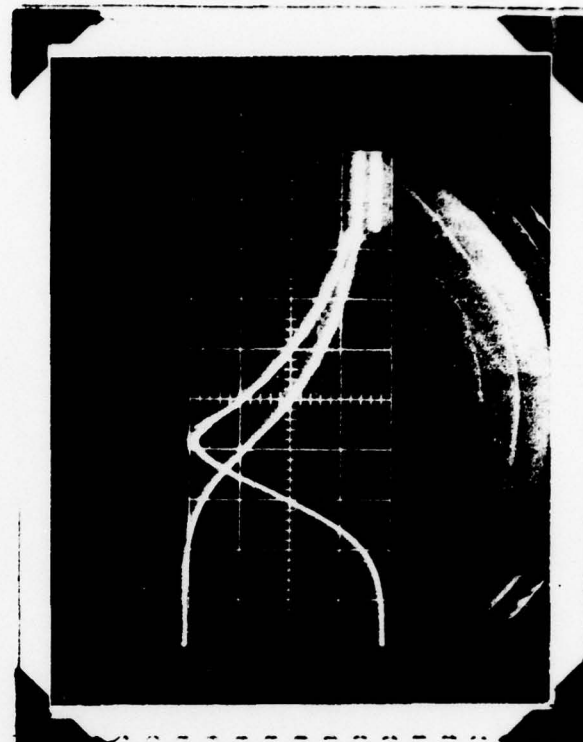
Signal __Voltage__   Signal __Current__
Ampl cm __2000 V__   Ampl/cm __400 m. a.__
Time cm __5 m. sec.__   Time/cm __5 m. sec.__

(8)

Fig. 5a.
cont'd.

Signal __Voltage__   Signal __Current__
Ampl/cm __1000 V__   Ampl/cm __200 m. a.__
Time/cm __5 m. sec.__   Time/cm __5 m. a.__

(5)

Signal __Voltage__   Signal __Current__
Ampl cm __2000 V__   Ampl cm __400 m. a.__
Time cm __5 m. sec.__   Time/cm __5 m. sec.__

(7)

70

Signal Voltage p(Torr) Signal Current
Ampl/cm 1000 V 3 x 10⁻⁴ Ampl/cm 200 m.a.
Time/cm 5 m. sec. Time/cm 5 m. sec.

(10)

Fig. 5 a. Discharge Characteristics cont'd.
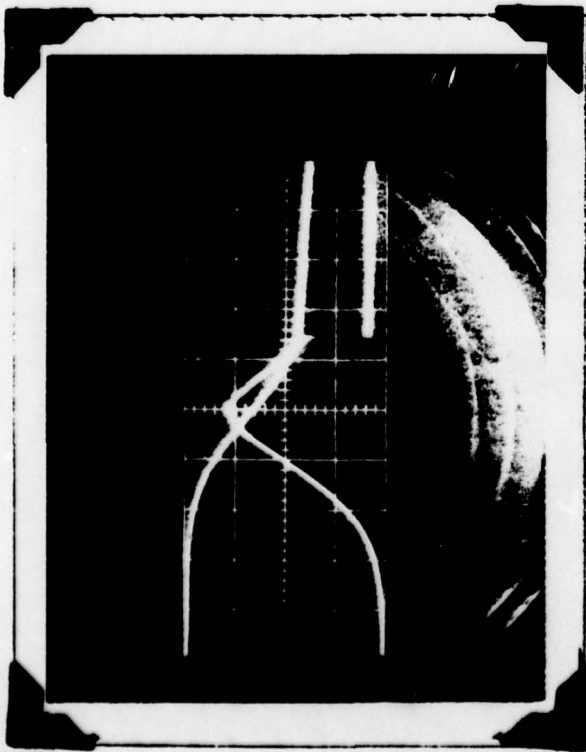
Signal Voltage p(Torr) Signal Current
Ampl/cm 1000 V 1 x 10⁻⁴ Ampl/cm 200 m.a.
Time/cm 5 m. sec. Time/cm 5 m. sec.

(9)
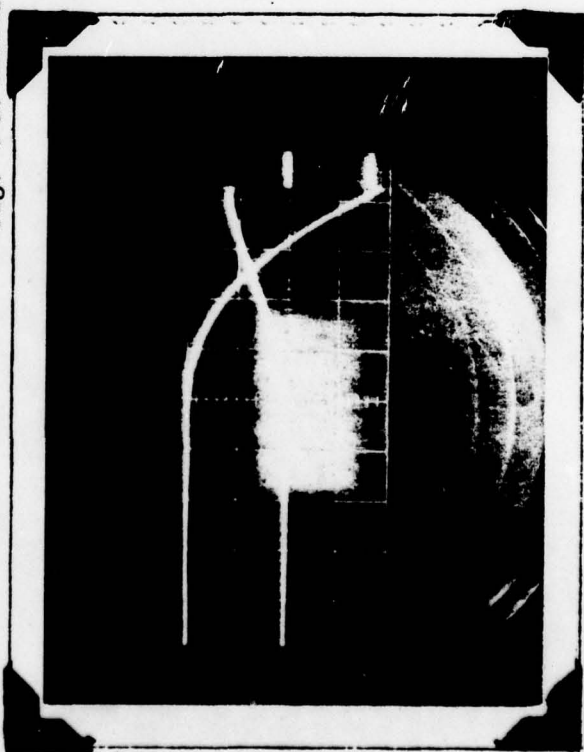
Signal Voltage p(Torr) Signal Current
Ampl/cm 1000 V 7 x 10⁻⁴ Ampl cm 1 Amp.
Time cm 5 m. sec. Time/cm 5 m. sec.

(11)

Signal Signal
Ampl/cm Ampl/cm
Time cm Time cm

71

FIG. 6 EXPERIMENTAL ARRANGEMENT IN VACUUM CHAMBER AT CONVAIR

72
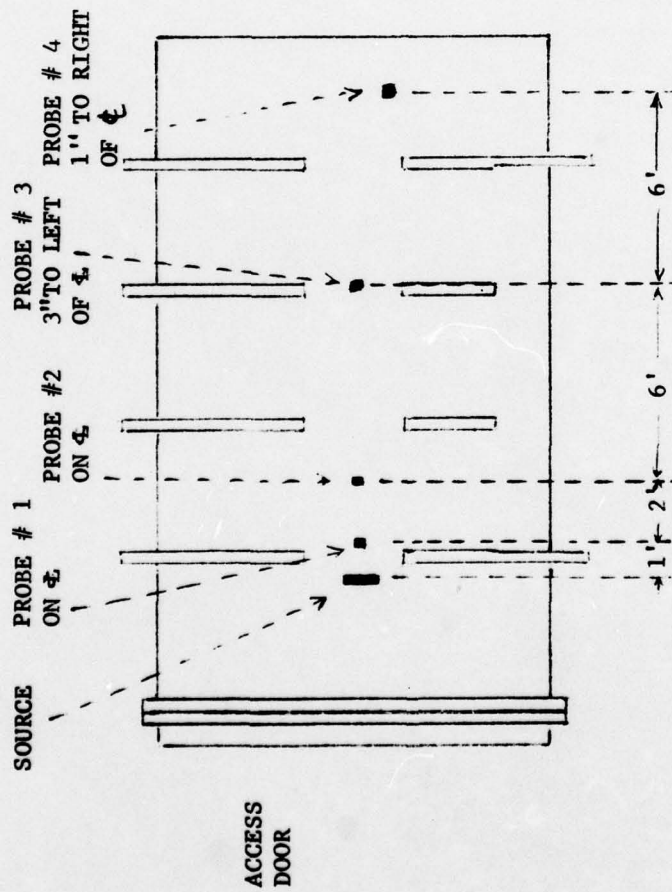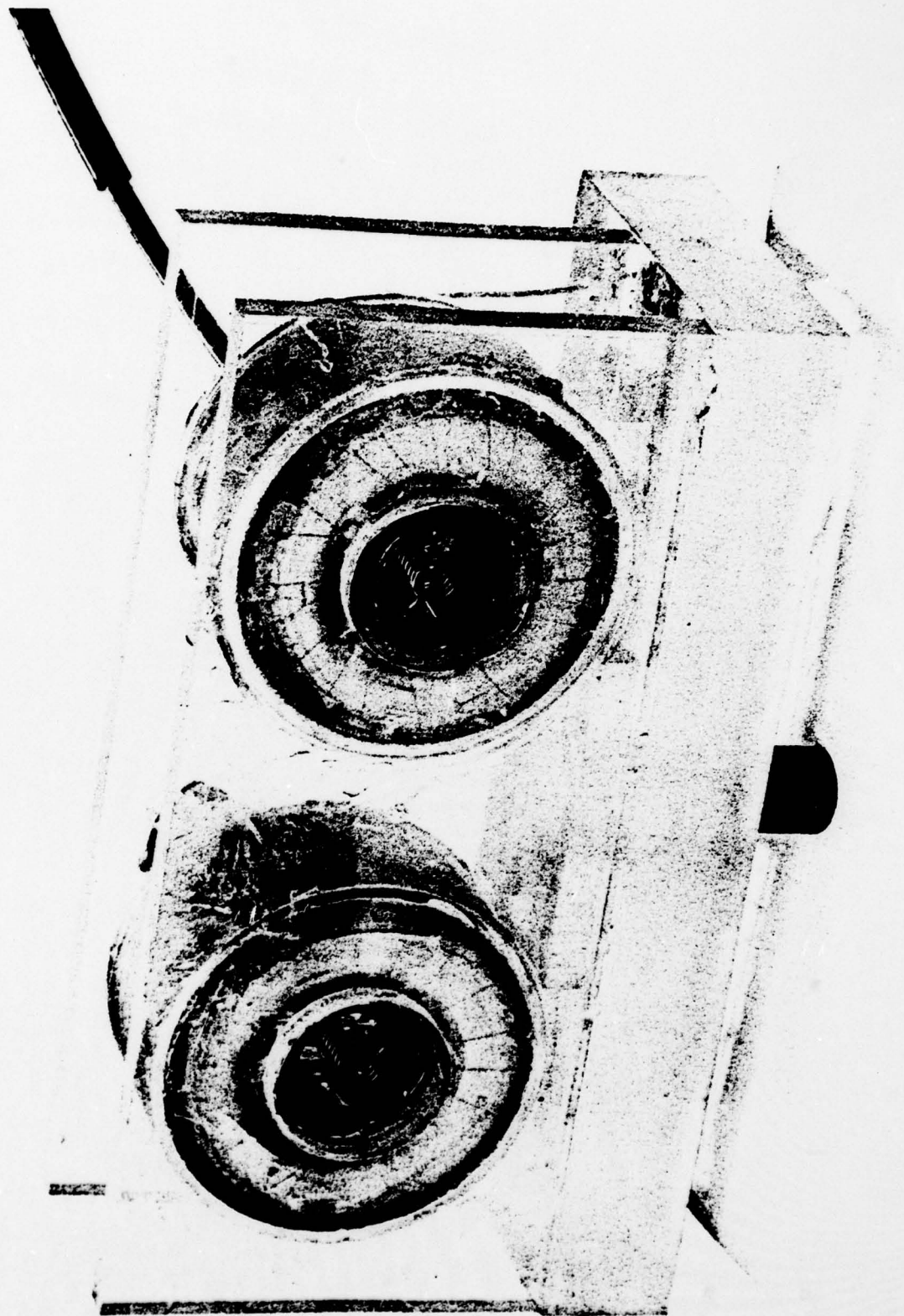
Figure 7   Photograph of Dual Ion Sources

73
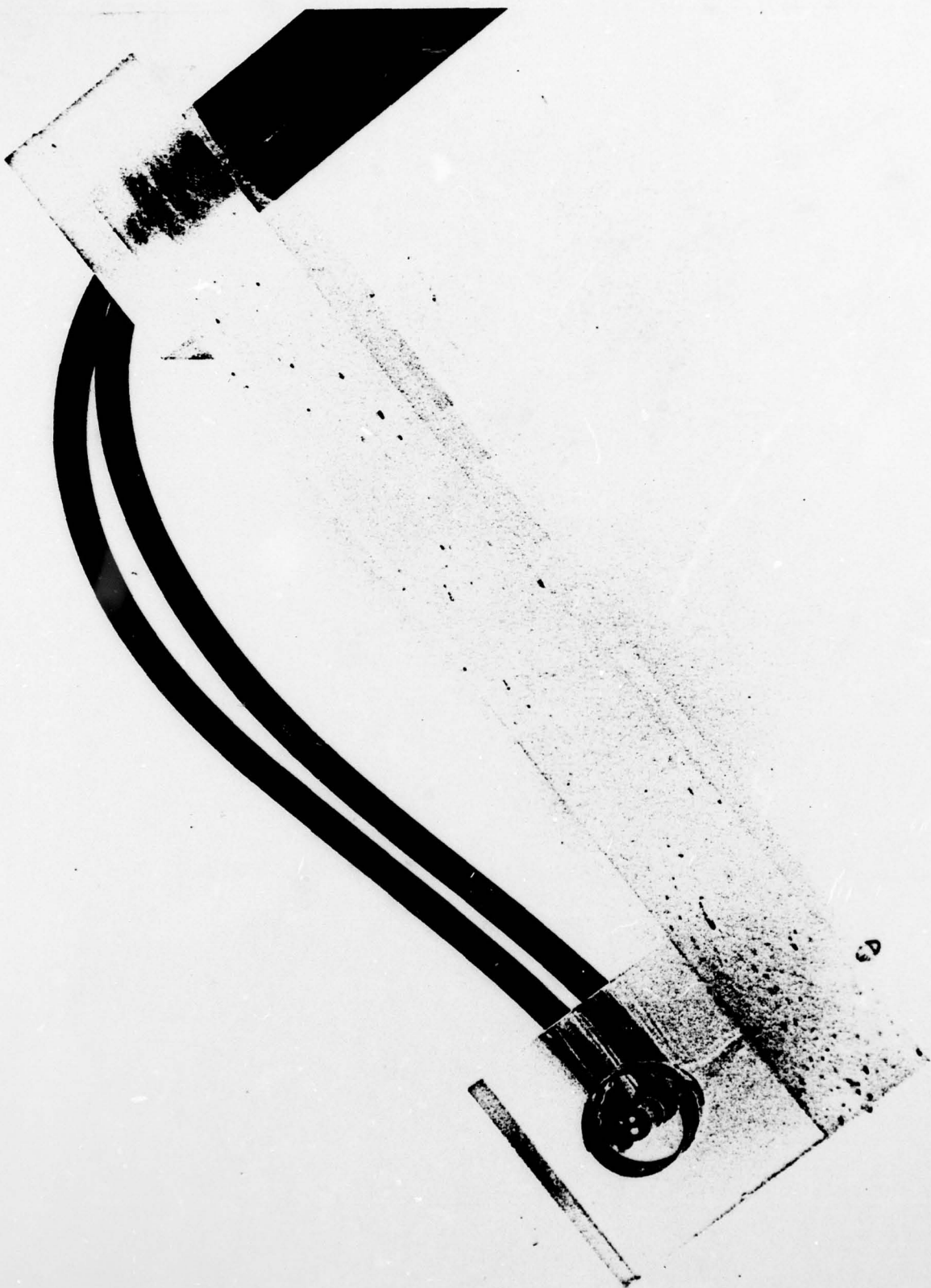
Figure 8 . Photograph of Ion Current Probe
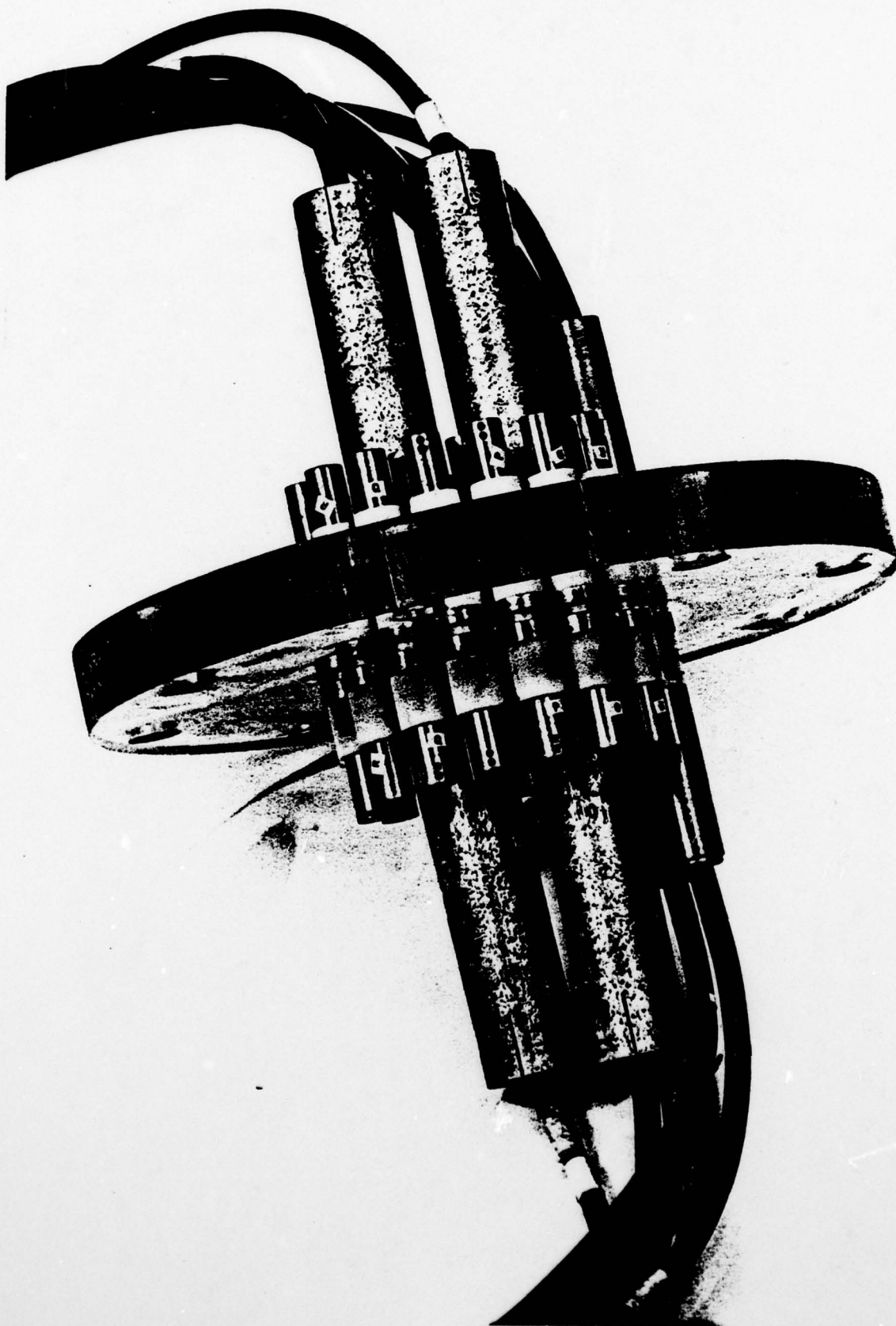
Figure 9   Photograph of Feed-Through Plate into Vacuum Chamber

CHARGING SWITCH

CHARGING RESISTOR

MAGNET POWER SUPPLY

$10^2 \, \Omega$

MAGNET

.06 f.

TO SCOPE INPUTS

100 AMP. CURRENT SHUNT

MAGNET CURRENT SIGNAL

CHARGING SWITCH

$10^4 \, \Omega$ CHARGING RESISTOR

$10^9 \, \Omega$ VOLTAGE DIVIDING NETWORK

DISCHARGE POWER SUPPLY

DISCHARGE TUBE

DISCHARGE VOLTAGE SIGNAL

$.04 \, \mu.f.$

START SWITCH

100 AMP. CURRENT SHUNT

FILAMENT CURRENT SIGNAL

CHARGING SWITCH

.06 f.

$5 \, \Omega$ CURRENT SHUNT

DISCHARGE CURRENT SIGNAL

FILAMENT POWER SUPPLY

FIG.10 SCHEMATIC OF DISCHARGE TUBE ELECTRIC CIRCUIT.

76

DETECTOR

8 μ.f.

10^4

10^5

10^6

SCALE
SELECTOR
SWITCH

0 TO 2000 V
D.C. POWER SUPPLY

$10^4 \Omega$

CHARGING
SWITCH

CHARGING
RESISTOR

$10^6 \Omega$ $10^6 \Omega$

SCOPE
INPUT
IMPEDANCE

TO DIFFERENTIAL
AMPLIFIER OF SCOPE
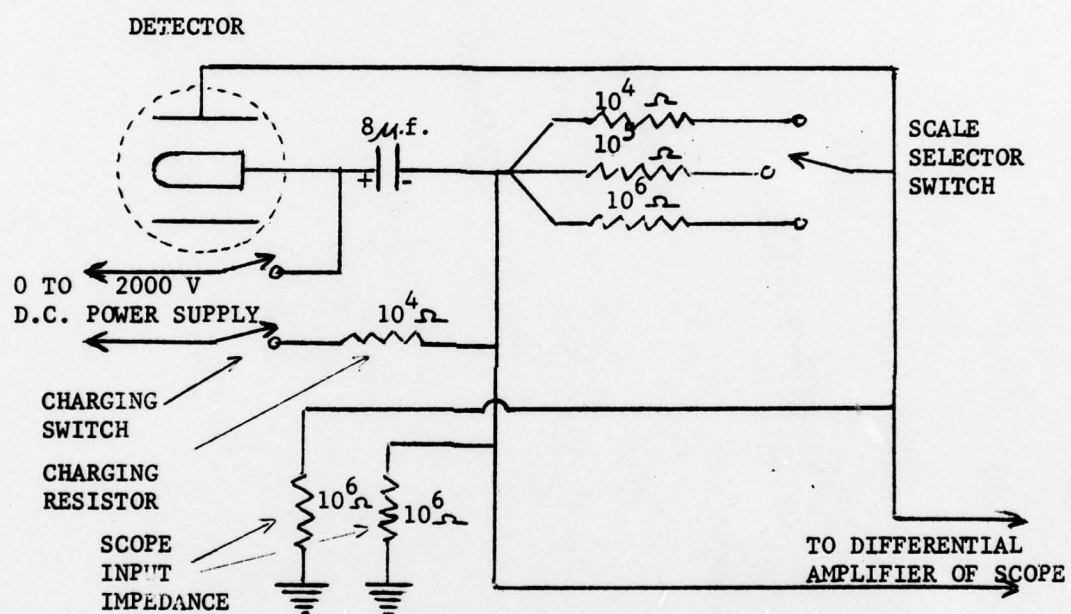
FIG. 11 SCHEMATIC OF DETECTOR CIRCUIT.

Date ___1-29-75___   Experiment _____

Picture # __1__
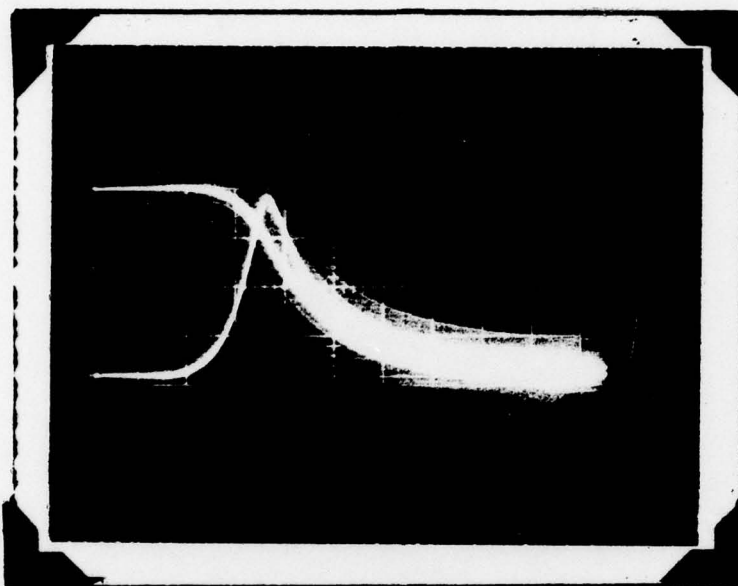
Capacitor Charging Voltages

Upper Detector _____ V
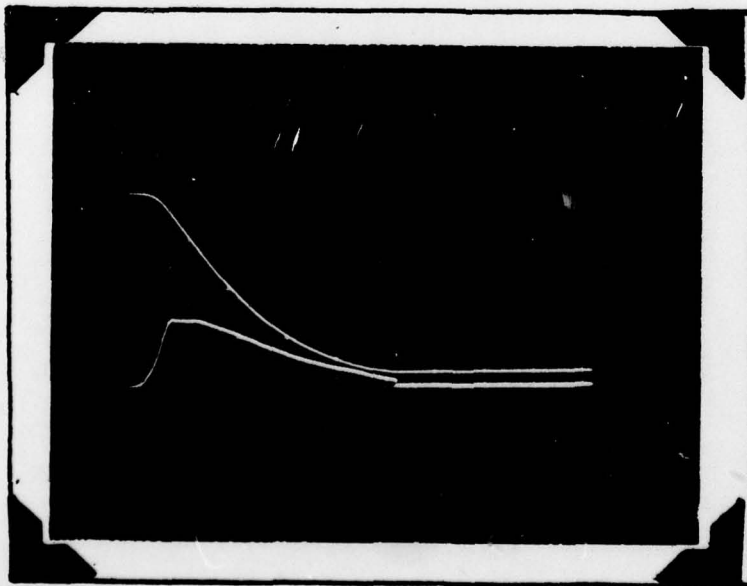Lower Detector _____ V
Discharge __2,000__ V
Filament ___35___ V
Magnet ___0___ V

Upper Trace

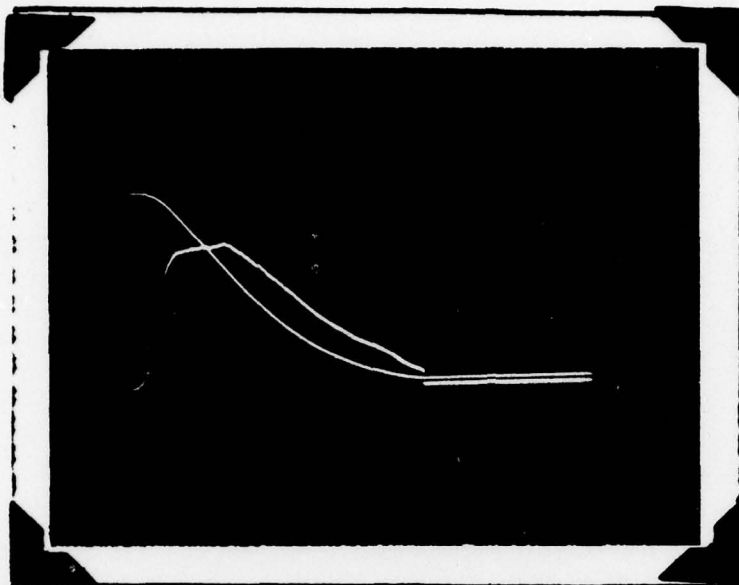Signal   Discharge Voltage
Ampl/cm.   500 V
Time/cm.   20 m. sec.

Lower Trace

Signal   Discharge Current
Ampl/cm.   100 m.a.
Time/cm.   10 m. sec.

Discharge Capacitor _4 μf._
Pressure = _6.0 x 10^{-7}_ Torr.

Figure 12a. Characteristic Current Voltage Traces —
             Applied Magnetic Field.
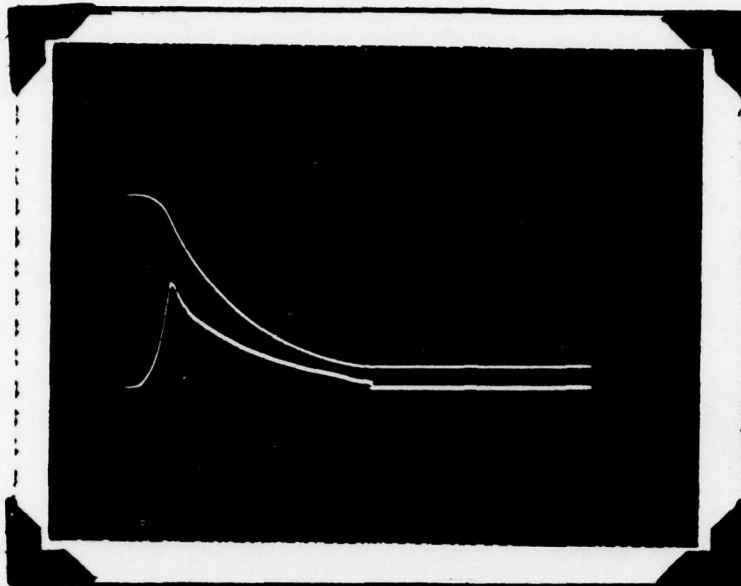
Picture # 2

Capacitor Charging Voltages

Upper Detector		V
Lower Detector		V
Discharge	2,000	V
Filament	35	V
Magnet	10	V

Upper Trace

Signal	Discharge Voltage
Ampl/cm.	500 V
Time/cm.	20 m. sec.

Lower Trace

Signal	Discharge Current
Ampl/cm.	100 m.a.
Time/cm.	20 m. sec.

Discharge Capacitor $\quad 4 \; \mu f$

Pressure = 6.0×10^{-7} Torr.

Picture # 3

Capacitor Charging Voltages

Upper Detector		V
Lower Detector		V
Discharge	2,000	V
Filament	35	V
Magnet	$12\frac{1}{2}$	V

Upper Trace

Signal	Discharge Voltage
Ampl/cm.	500 V
Time/cm.	20 m. sec.

Lower Trace

Signal	Discharge Current
Ampl/cm.	100 m.a.
Time/cm.	20 m. sec.

Discharge Capacitor $\quad 4 \; \mu f$

Pressure = 6.0×10^{-7} Torr.

Figure 12b   (Continued)

Picture #__4__

Capacitor Charging Voltages

Upper Detector _____ V
Lower Detector _____ V
Discharge __2,000__ V
Filament ____35____ V
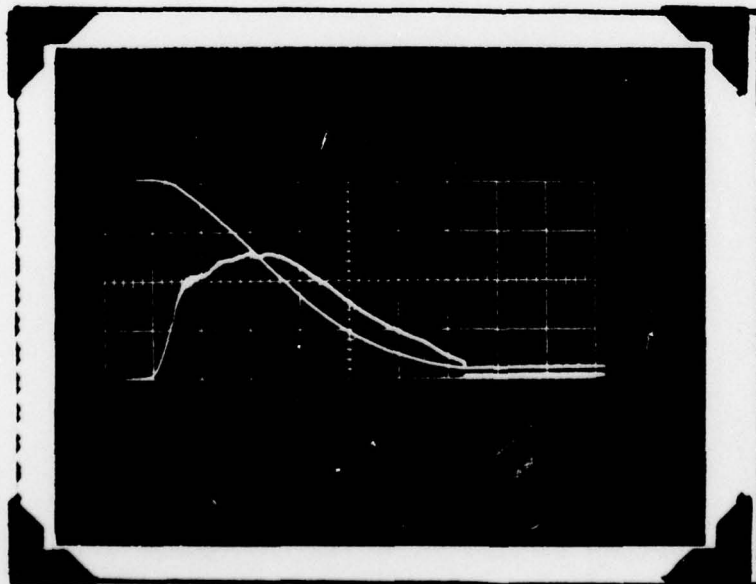Magnet ____15____ V

Upper Trace

Signal   Discharge Voltage
Ampl/cm.   500 V
Time/cm.   20 m. sec.

Lower Trace

Signal   Discharge Current
Ampl/cm.   40 m.a.
Time/cm.   20 m. sec.

Discharge Capacitor __4__ μf
Pressure = _6.0 x 10^{-7}_ Torr.

Picture #__5__

Capacitor Charging Voltages

Upper Detector _____ V
Lower Detector _____ V
Discharge __2,000__ V
Filament ____35____ V
Magnet __17½__ V

Upper Trace

Signal   Discharge Voltage
Ampl/cm.   500 V
Time/cm.   20 m. sec.

Lower Trace

Signal   Discharge Current
Ampl/cm.   40 m.a.
Time/cm.   20 m. sec.

Discharge Capacitor __4__ μf
Pressure = _6.0 x 10^{-7}_ Torr.

Figure 12c   (Continued)

Date _____ 1-29-75 _____   Experiment _____
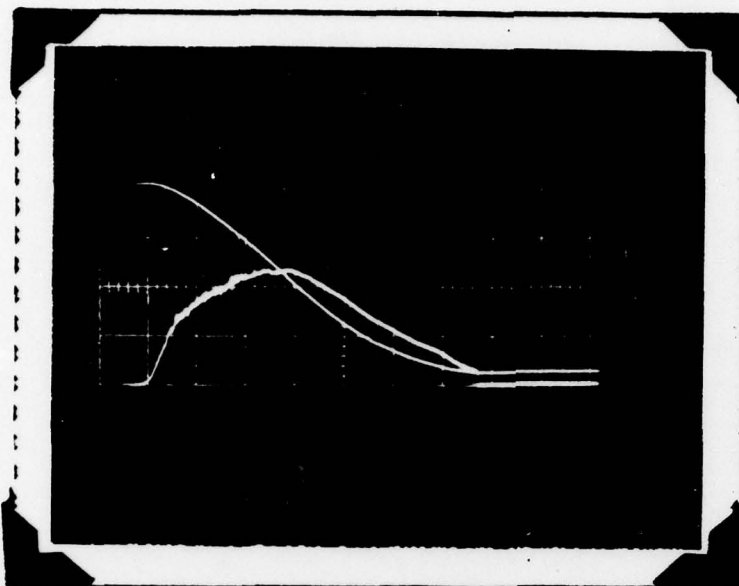
Picture # __6__

Capacitor Charging Voltages

Upper Detector	_____	V
Lower Detector	_____	V
Discharge	2,000	V
Filament	35	V
Magnet	20	V

Upper Trace

Signal	Discharge Voltage
Ampl/cm.	500 V
Time/cm.	20 m. sec.

Lower Trace

Signal	Discharge Current
Ampl/cm.	40 m.a.
Time/cm.	20 m. sec.

Discharge Capacitor __4 μf__

Pressure = __6.0 x 10^{-7}__ Torr.

Picture # __7__

Capacitor Charging Voltages

Upper Detector	_____	V
Lower Detector	_____	V
Discharge	2,000	V
Filament	35	V
Magnet	22½	V

Upper Trace

Signal	Discharge Voltage
Ampl/cm.	500 V
Time/cm.	20 m. sec.

Lower Trace

Signal	Discharge Current
Ampl/cm.	40 m.a.
Time/cm.	20 m. sec.

Discharge Capacitor __4 μf__

Pressure = __6.0 x 10^{-7}__ Torr.

Figure 12d   (Continued)
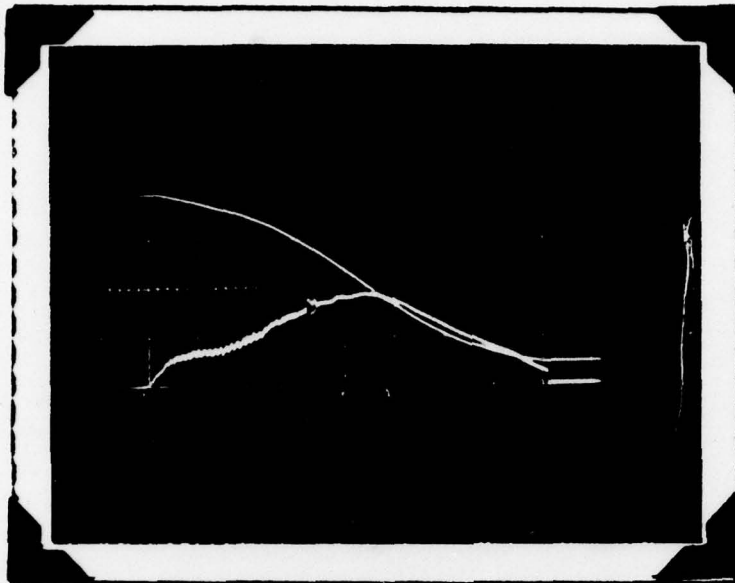
81

Picture # 10

Capacitor Charging Voltages

Upper Detector _____ V
Lower Detector _____ V
Discharge   2,000   V
Filament   35   V
Magnet   30   V

Upper Trace

Signal   Discharge Voltage
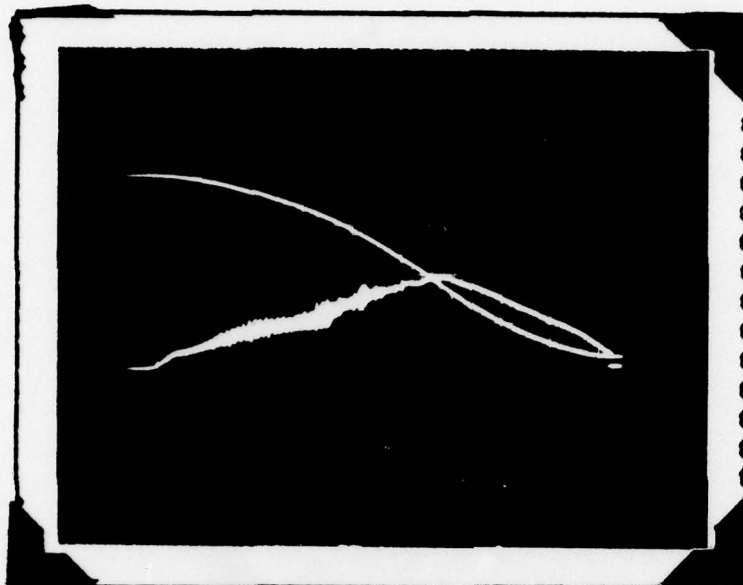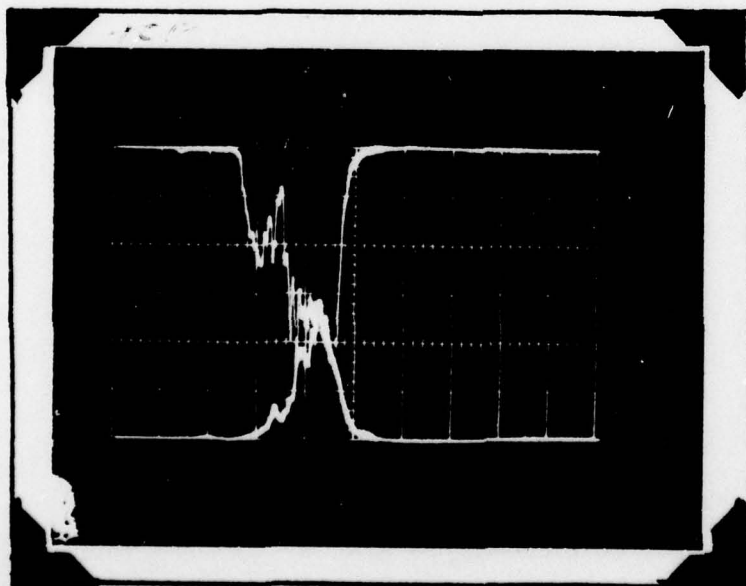Ampl/cm.   500 V
Time/cm.   20 m. sec.

Lower Trace

Signal   Discharge Current
Ampl/cm.   40 m.a.
Time/cm.   20 m. sec.

Discharge Capacitor 4 μf.
Pressure = 6.0 x 10⁻⁷ Torr.

Picture # 11

Capacitor Charging Voltages

Upper Detector _____ V
Lower Detector _____ V
Discharge   2,000   V
Filament   35   V
Magnet   32½   V

Upper Trace

Signal   Discharge Voltage
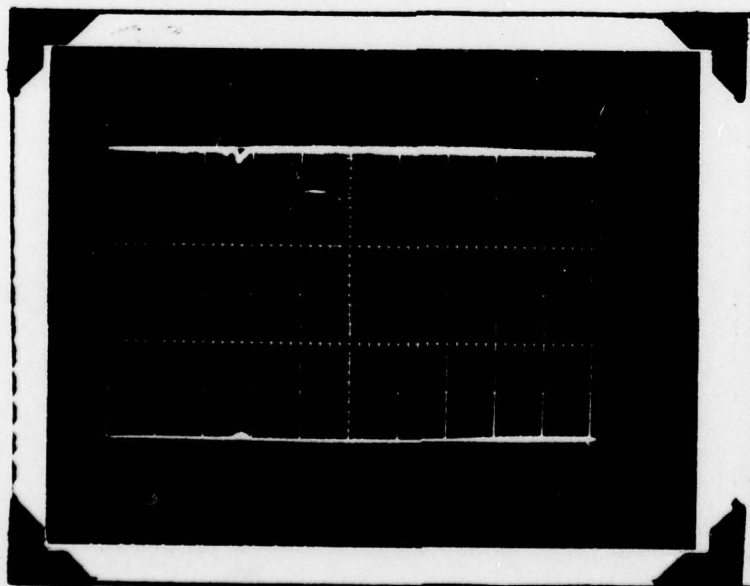Ampl/cm.   500 V
Time/cm.   20 m. sec.

Lower Trace

Signal   Discharge Current
Ampl/cm.   40 m.a.
Time/cm.   20 m. sec.

Discharge Capacitor 4 μf.
Pressure = 6.0 x 10⁻⁷ Torr.

Figure 12e   (Continued)

Picture #_62A_

Capacitor Charging Voltages

Upper Detector _____ V
Lower Detector _____ V
Discharge ___2.000___ V
Filament ___35___ V
Magnet ___45___ V

Upper Trace

Signal ___Discharge Voltage___
Ampl/cm. ___500 V___
Time/cm. ___20 m. sec.___

Lower Trace

Signal ___Discharge Current___
Ampl/cm. ___40 m a.___
Time/cm. ___20 m. sec___

Discharge Capacitor _4_ μf.
Pressure = 6.0 x 10^{-7} Torr.

Picture #_62B_

Capacitor Charging Voltages

Upper Detector ___1.000___ V
Lower Detector ___1.000___ V
Discharge ___2.000___ V
Filament ___35___ V
Magnet ___45___ V

Upper Trace

Signal ___Detector 3___
Ampl/cm. ___100 mV___
Time/cm. ___20 m. sec.___

Lower Trace

Signal ___Detector 4___
Ampl/cm. ___500 mV___
Time/cm. ___20 m. sec.___

Discharge Capacitor _4_ μf.
Pressure = 6.0 x 10^{-7} Torr.

Figure 12f   (Continued)

Date ___1-29-75___   Experiment _____

Picture #__64 A__

Capacitor Charging Voltages

Upper Detector	_____	V
Lower Detector	_____	V
Discharge	2,000	V
Filament	35	V
Magnet	47½	V

Upper Trace

Signal	Discharge Voltage
Ampl/cm.	500 V
Time/cm.	20 m. sec.

Lower Trace

Signal	Discharge Current
Ampl/cm.	40 m.a.
Time/cm.	20 m. sec.

Discharge Capacitor 4 μf

Pressure = 6.0 x 10^{-7} Torr.

40 m. sec. delay

Picture #__64 B__

Capacitor Charging Voltages

Upper Detector	1,000	V
Lower Detector	1,000	V
Discharge	2,000	V
Filament	35	V
Magnet	47½	V

Upper Trace

Signal	Detector 3
Ampl/cm.	100 mV
Time/cm.	20 m. sec.

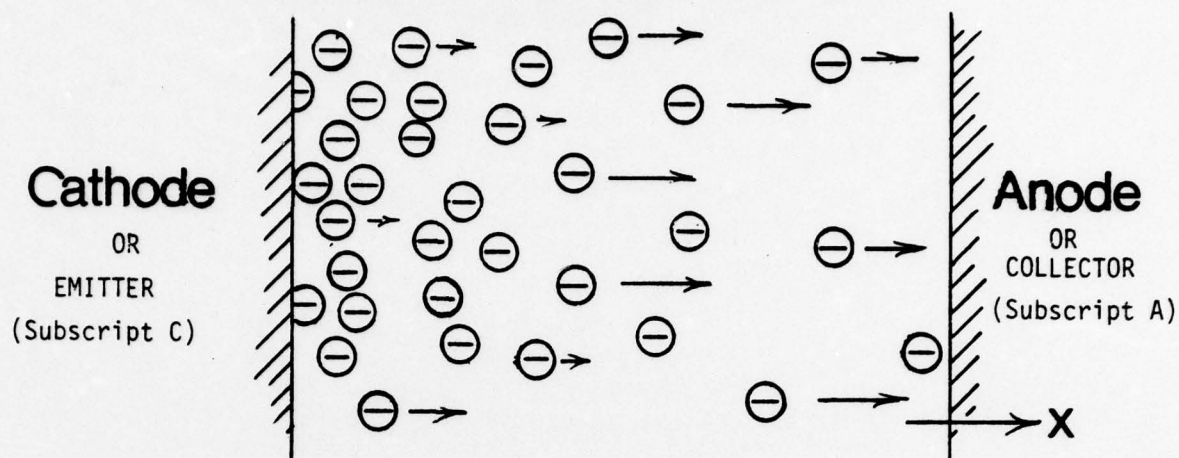Lower Trace

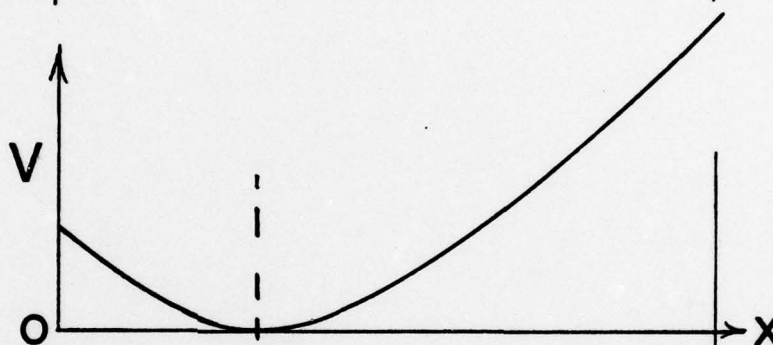|	
Signal	Detector 4
Ampl/cm.	500 mV
Time/cm.	20 m. sec.

Discharge Capacitor 4 μf

Pressure = 6.0 x 10^{-7} Torr.

40 m. sec. delay

Figure 12g   (Continued)

84

FIGURE 13
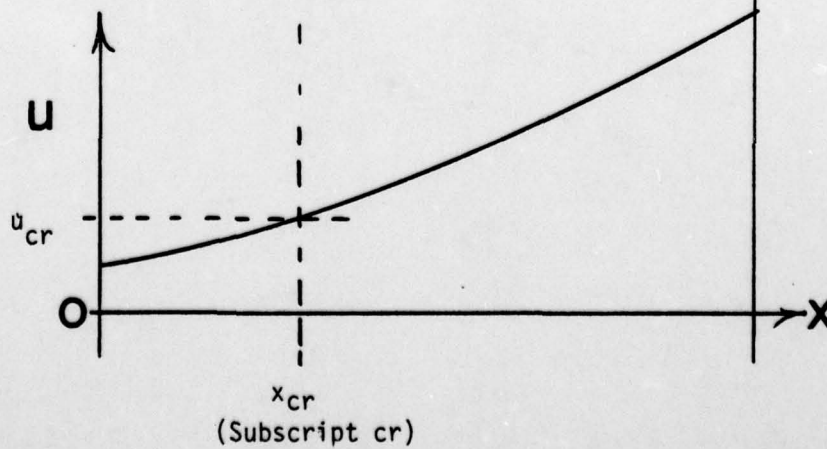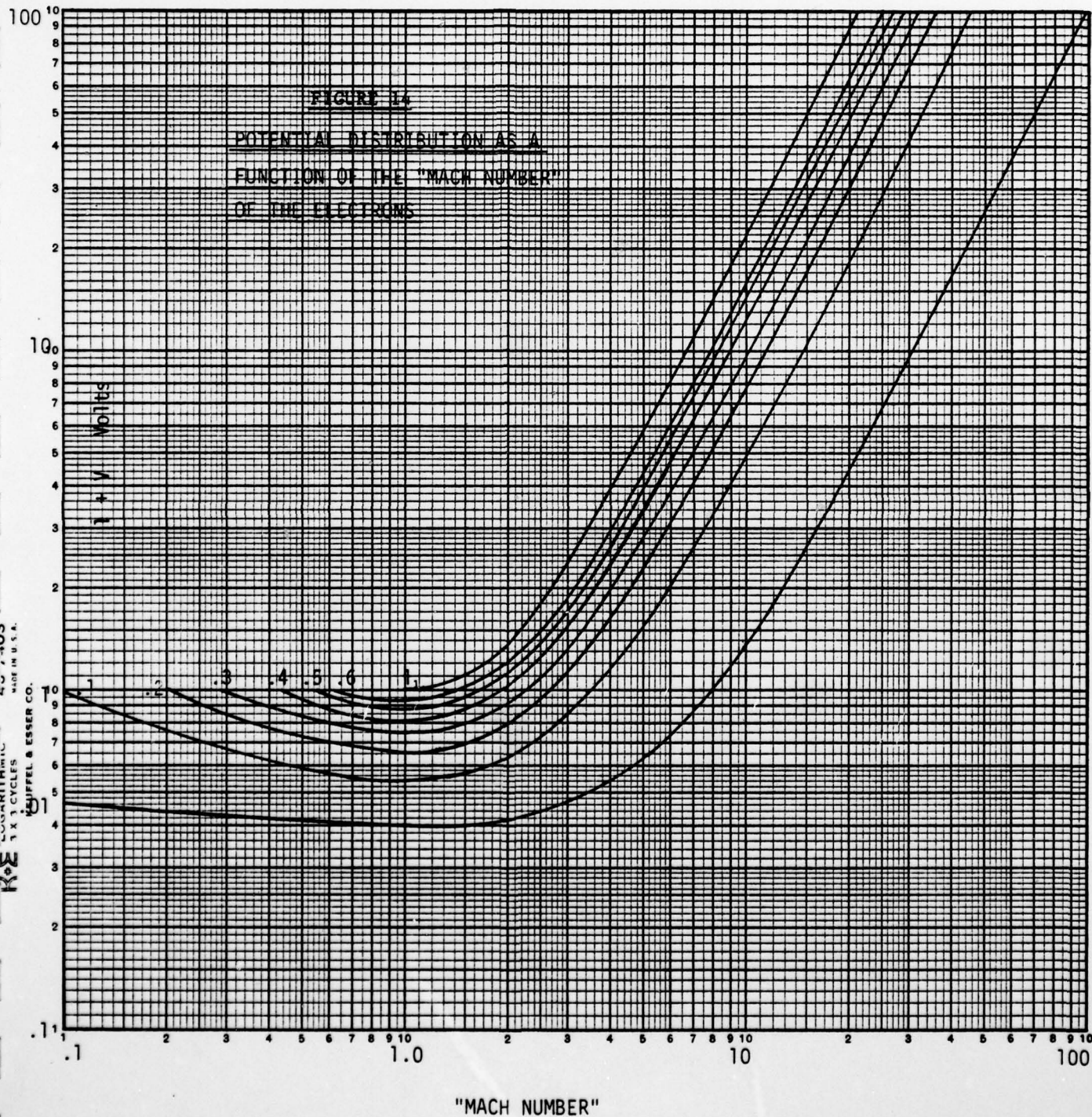SCHEMATIC OF GEOMETRIC AND ELECTRIC CONFIGURATION

Cathode
OR
EMITTER
(Subscript C)

Anode
OR
COLLECTOR
(Subscript A)

V

POTENTIAL
DISTRIBUTION

O

X

ELECTRIC FIELD
DISTRIBUTION

$E_x = -\dfrac{dV}{dx}$

O

X

ELECTRON VELOCITY
DISTRIBUTION
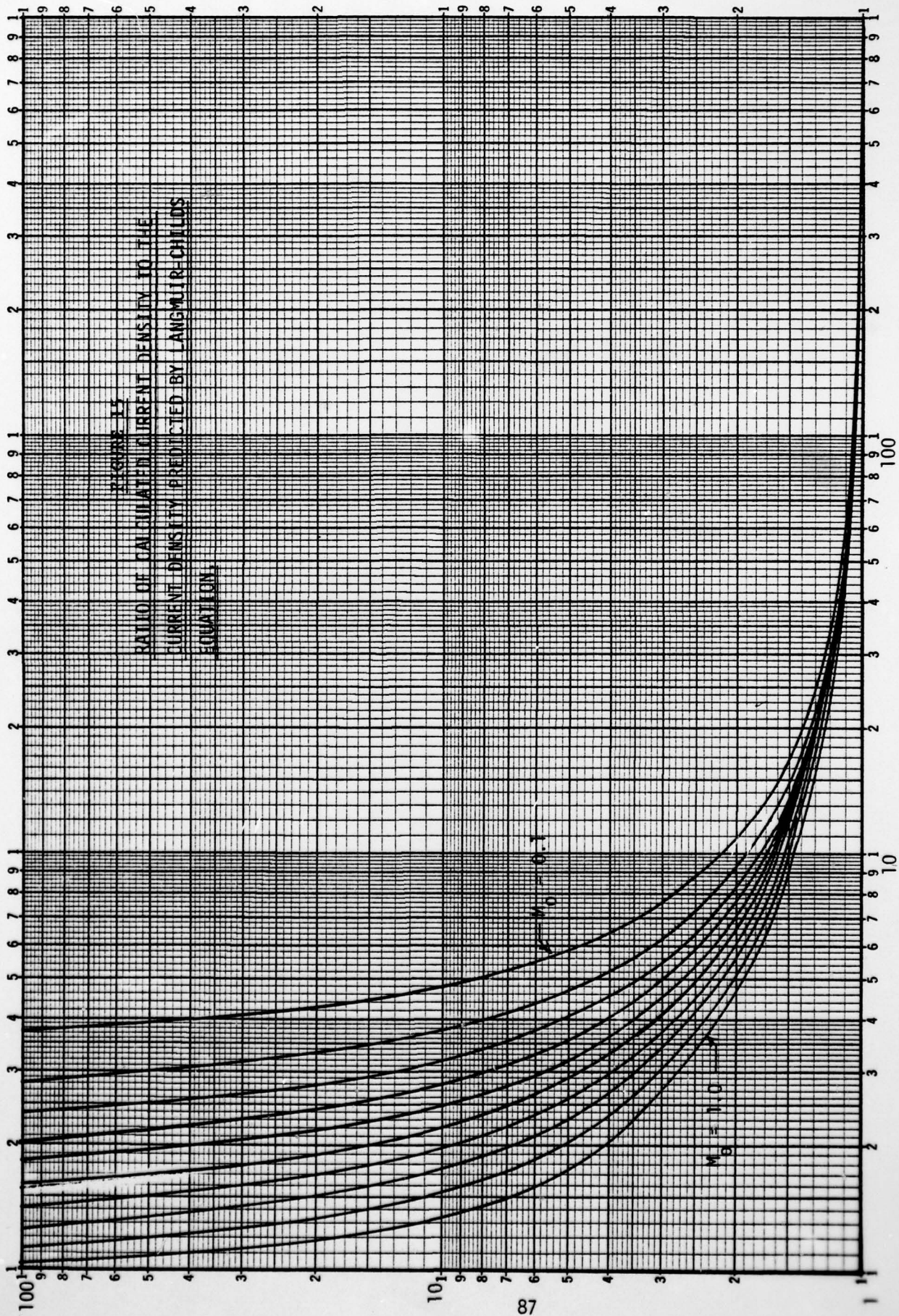
u

u_{cr}

O

X

x_{cr}
(Subscript cr)

85

FIGURE 14

POTENTIAL DISTRIBUTION AS A
FUNCTION OF THE "MACH NUMBER"
OF THE ELECTRONS

"MACH NUMBER"

FIGURE 15

RATIO OF CALCULATED CURRENT DENSITY TO THE CURRENT DENSITY PREDICTED BY LANGMUIR-CHILDS EQUATION.

"MACH NUMBER"

$M_\beta = 0.1$

$M_\beta = 1.0$

$\frac{\Phi^*}{\Phi} = 10$
$T = Z = 1$
$Y = 2.35563$
$\langle L, C \rangle = 2.5231$

$\frac{\Phi}{\Phi^*}$

$-\frac{d}{d\eta} \left(\frac{\Phi}{\Phi^*} \right)$

η
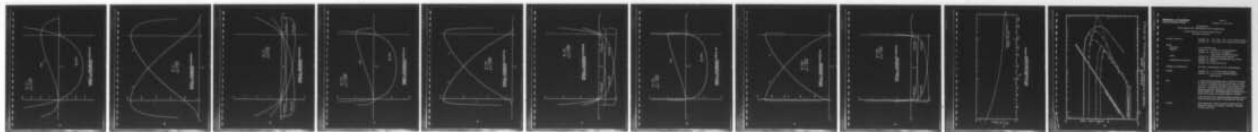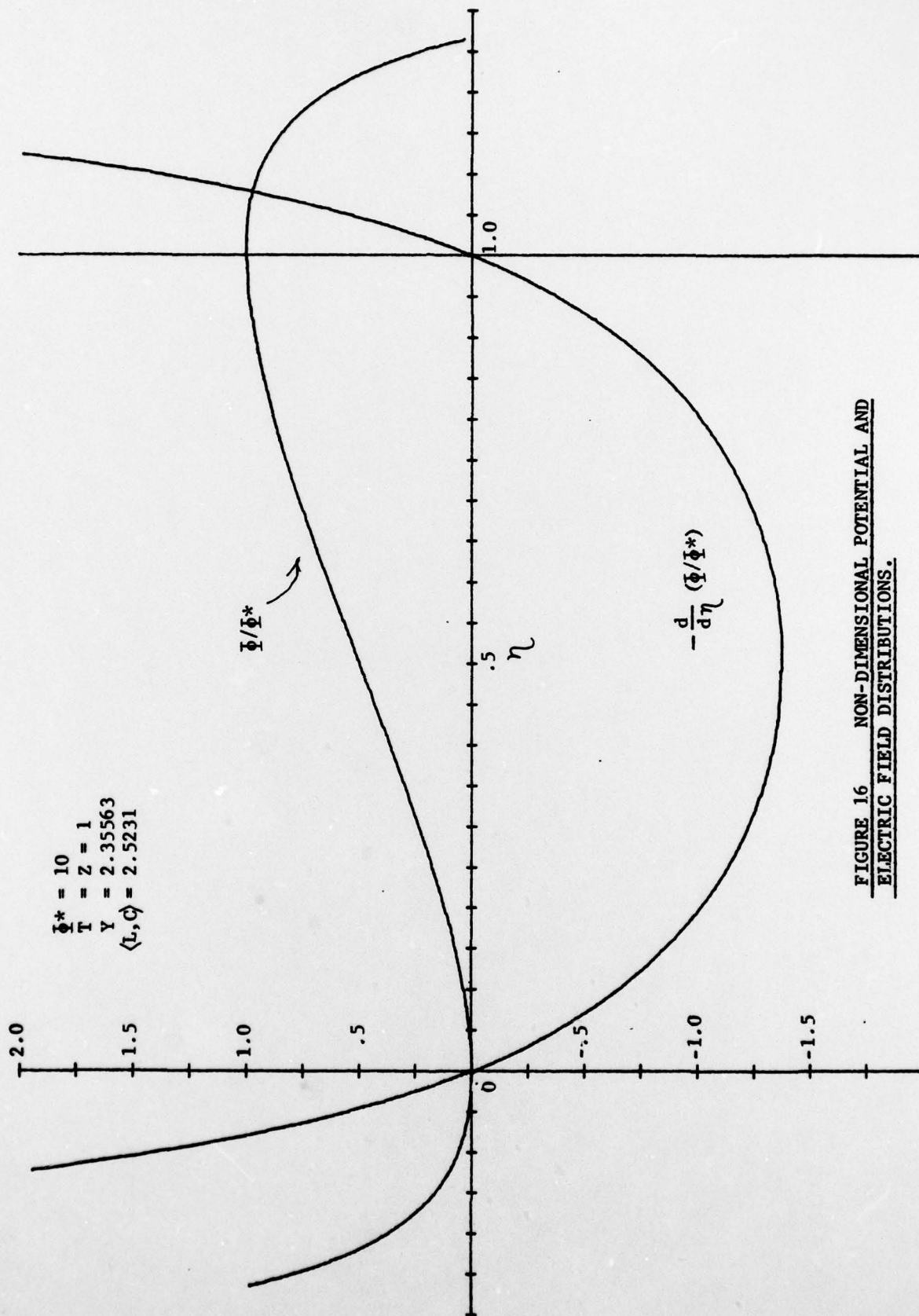
FIGURE 16   NON-DIMENSIONAL POTENTIAL AND
ELECTRIC FIELD DISTRIBUTIONS.

$\phi^* = 10$
$T = Z = 1$
$Y = 2.35563$
$\langle L, C \rangle = 2.5231$
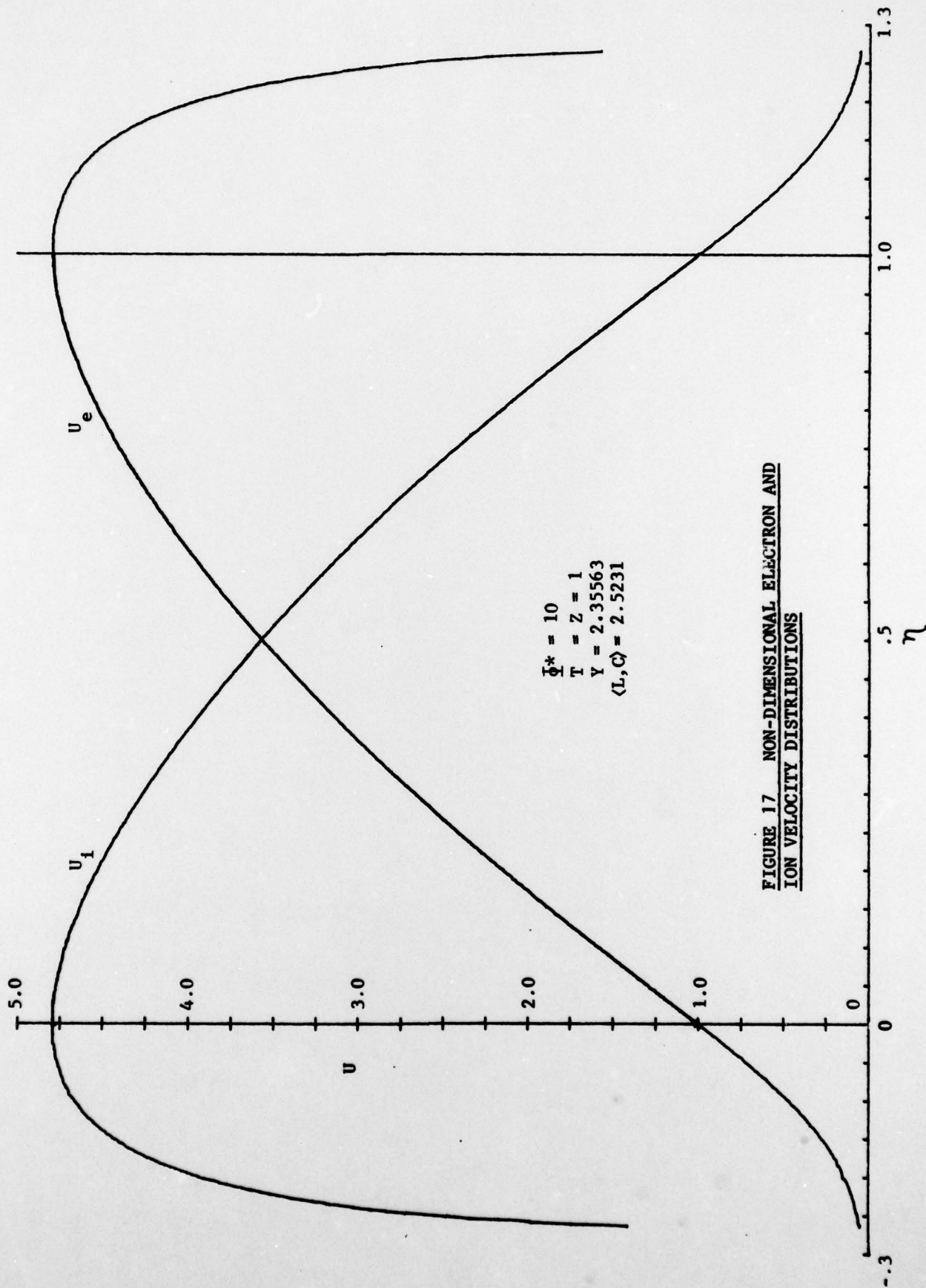
FIGURE 17 NON-DIMENSIONAL ELECTRON AND
ION VELOCITY DISTRIBUTIONS

$\frac{\Phi^*}{T} = 10$
$T = Z = 1$
$Y = 2.35563$
$\langle L, C \rangle = 2.5231$

$\log(T_e / T_e^{**})$

$\log(p_e / p_e^{**})$
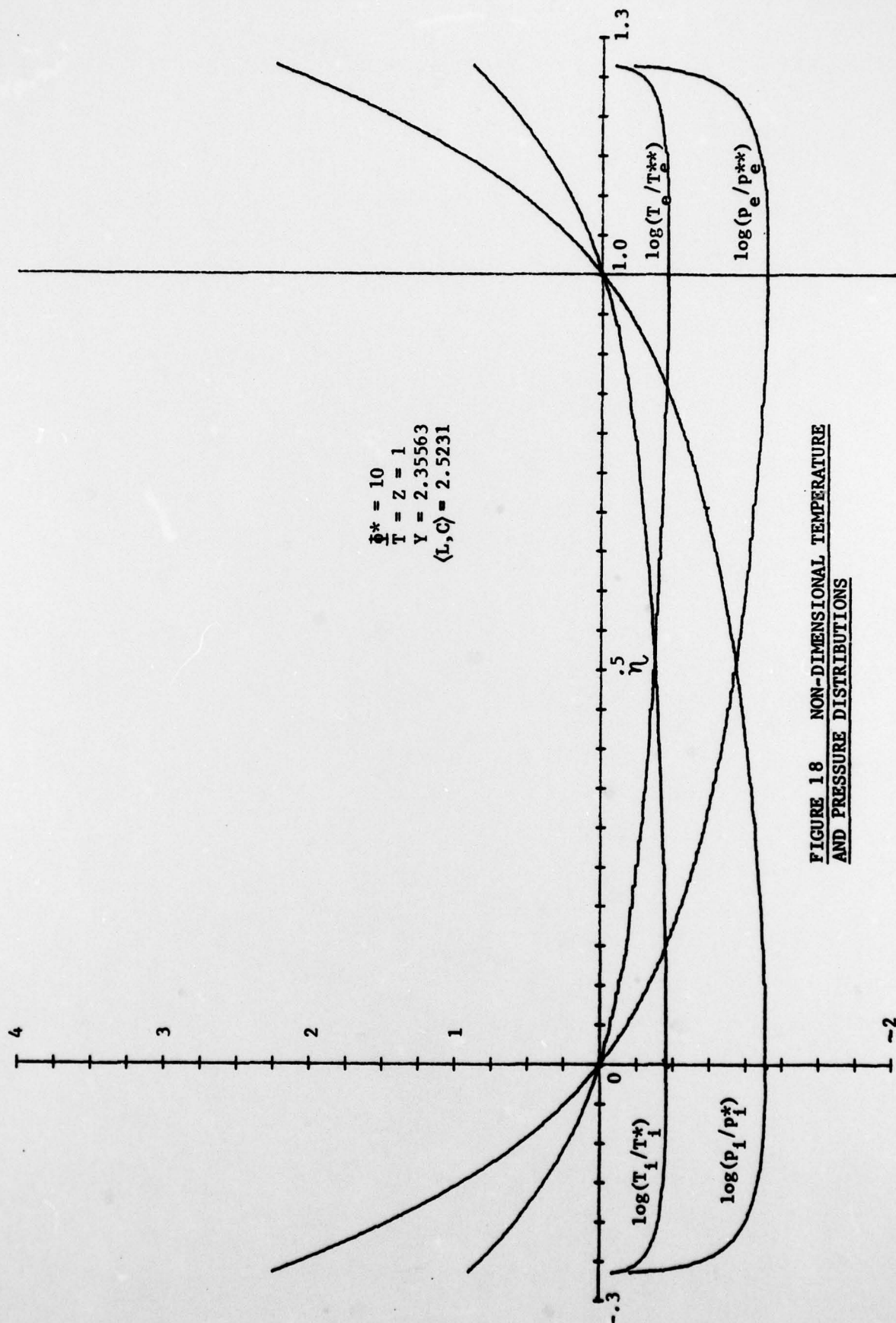
$\log(T_i / T_i^*)$

$\log(p_i / p_i^*)$

FIGURE 18   NON-DIMENSIONAL TEMPERATURE
AND PRESSURE DISTRIBUTIONS

90

$\frac{\Phi^*}{T} = .100$
$T = Z = 1$
$Y = 1.268262$
$\langle L, C \rangle = 1.27928$

Φ/Φ^*

$-\frac{d}{d\eta} (\Phi/\Phi^*)$

η

FIGURE 19 NON-DIMENSIONAL POTENTIAL AND
ELECTRIC FIELD DISTRIBUTIONS

91

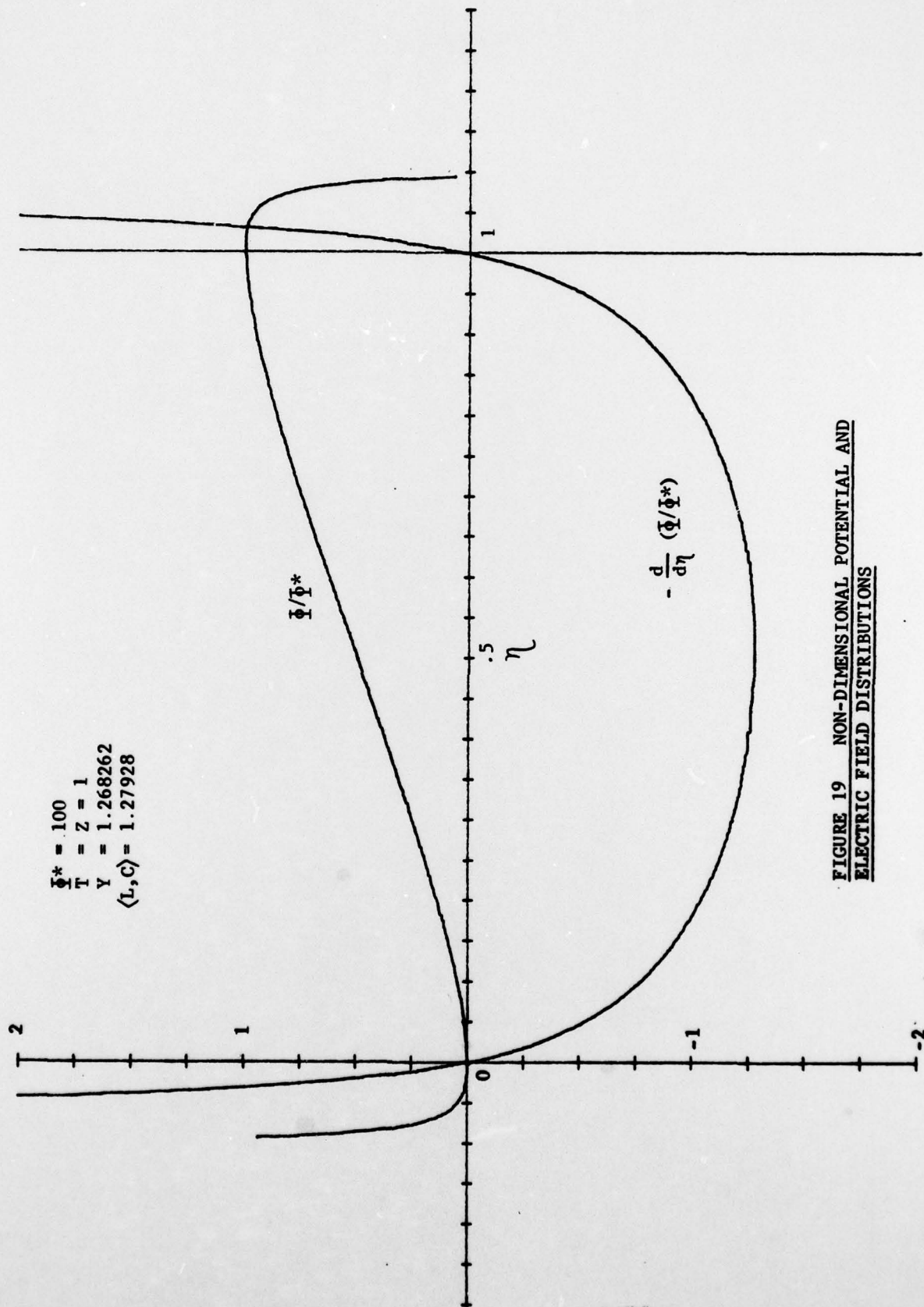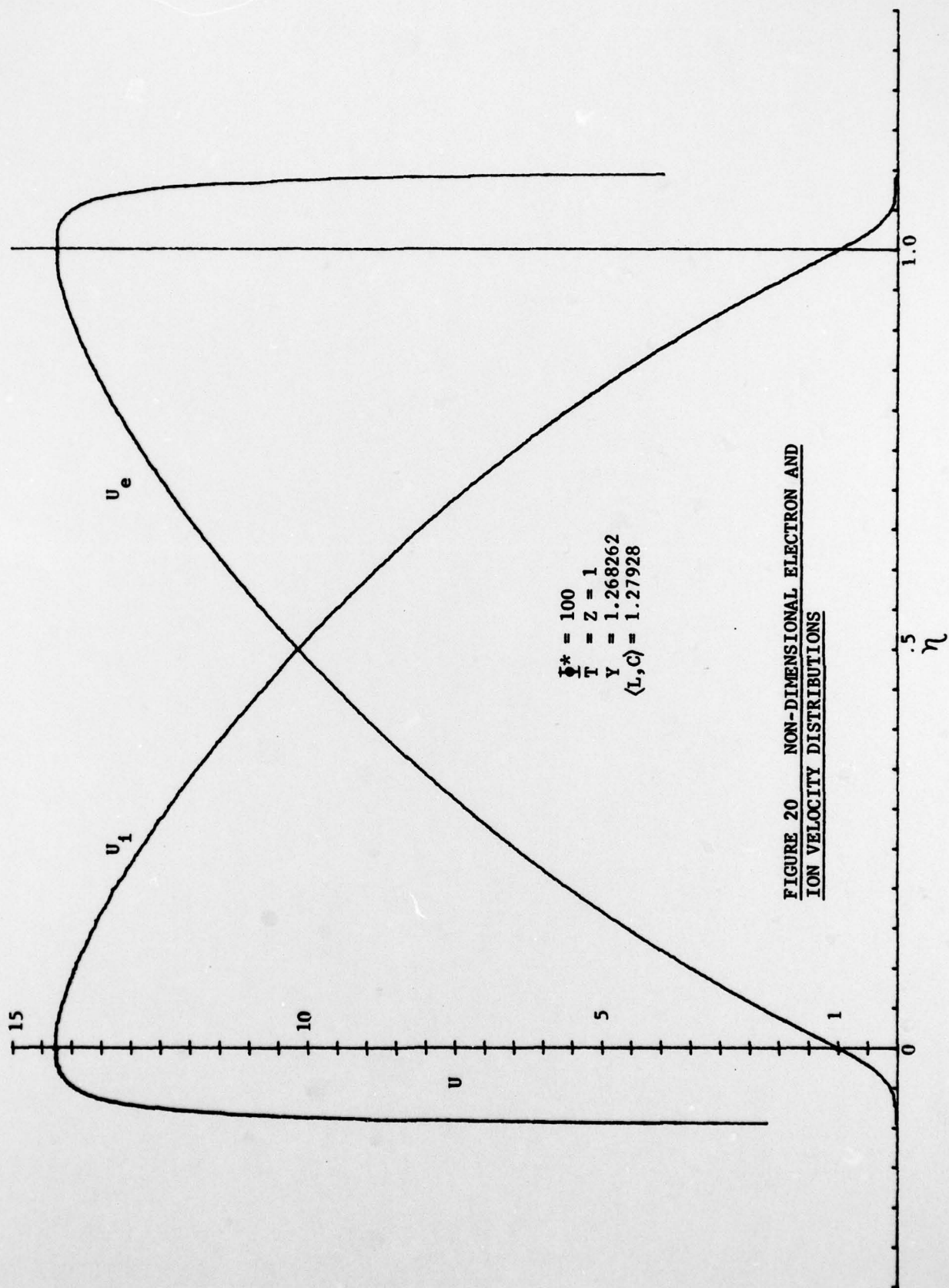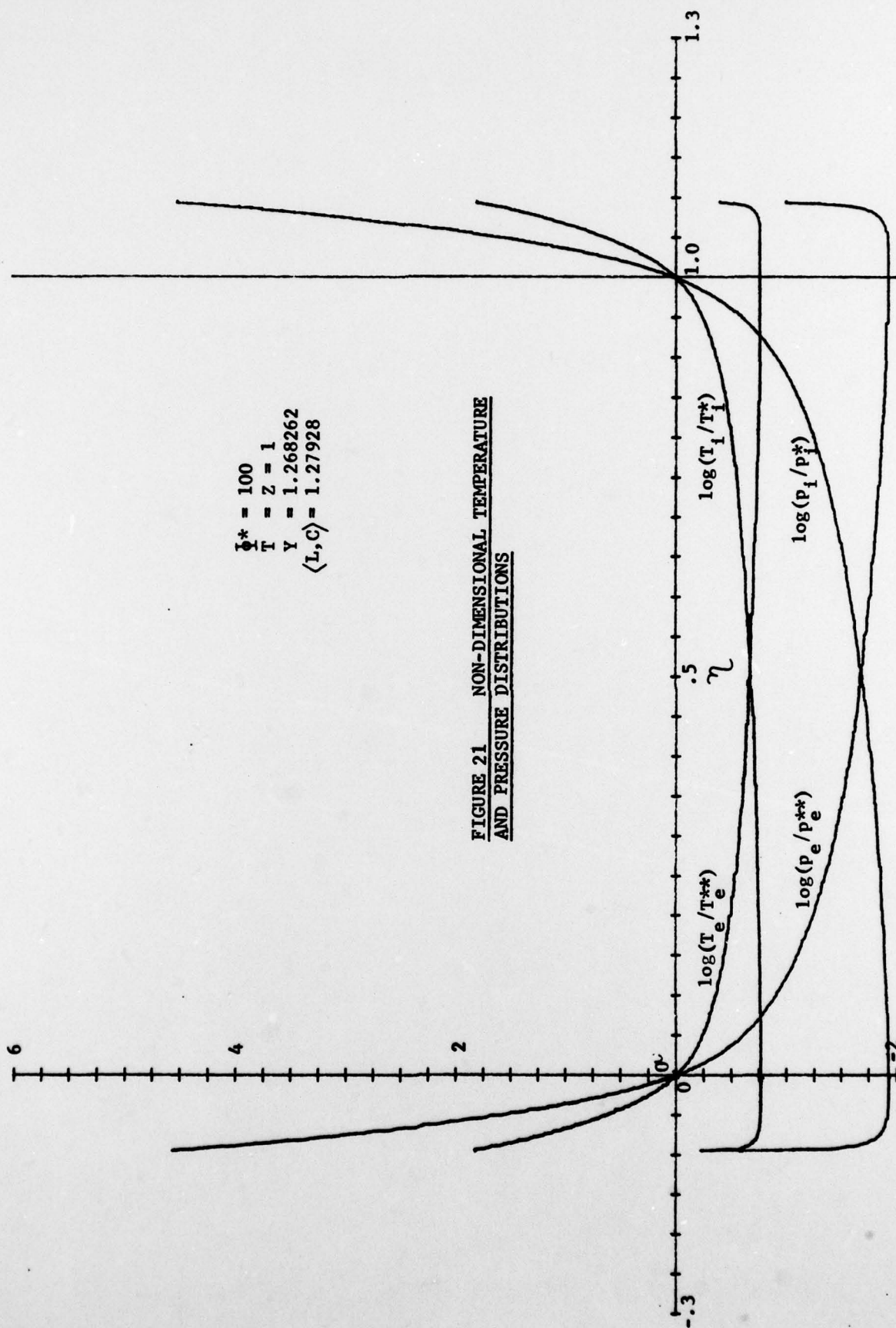FIGURE 20   NON-DIMENSIONAL ELECTRON AND
ION VELOCITY DISTRIBUTIONS

$\Phi^* = 100$
$T = Z = 1$
$Y = 1.268262$
$\langle L, C \rangle = 1.27928$

92

FIGURE 21   NON-DIMENSIONAL TEMPERATURE
AND PRESSURE DISTRIBUTIONS

$\phi^* = 100$
$T = Z = 1$
$Y = 1.268262$
$\langle L, C \rangle = 1.27928$

93

$\Phi^* = 1000$
$T = Z = 1$
$Y = .964378$
$\langle L, C \rangle = .965285$

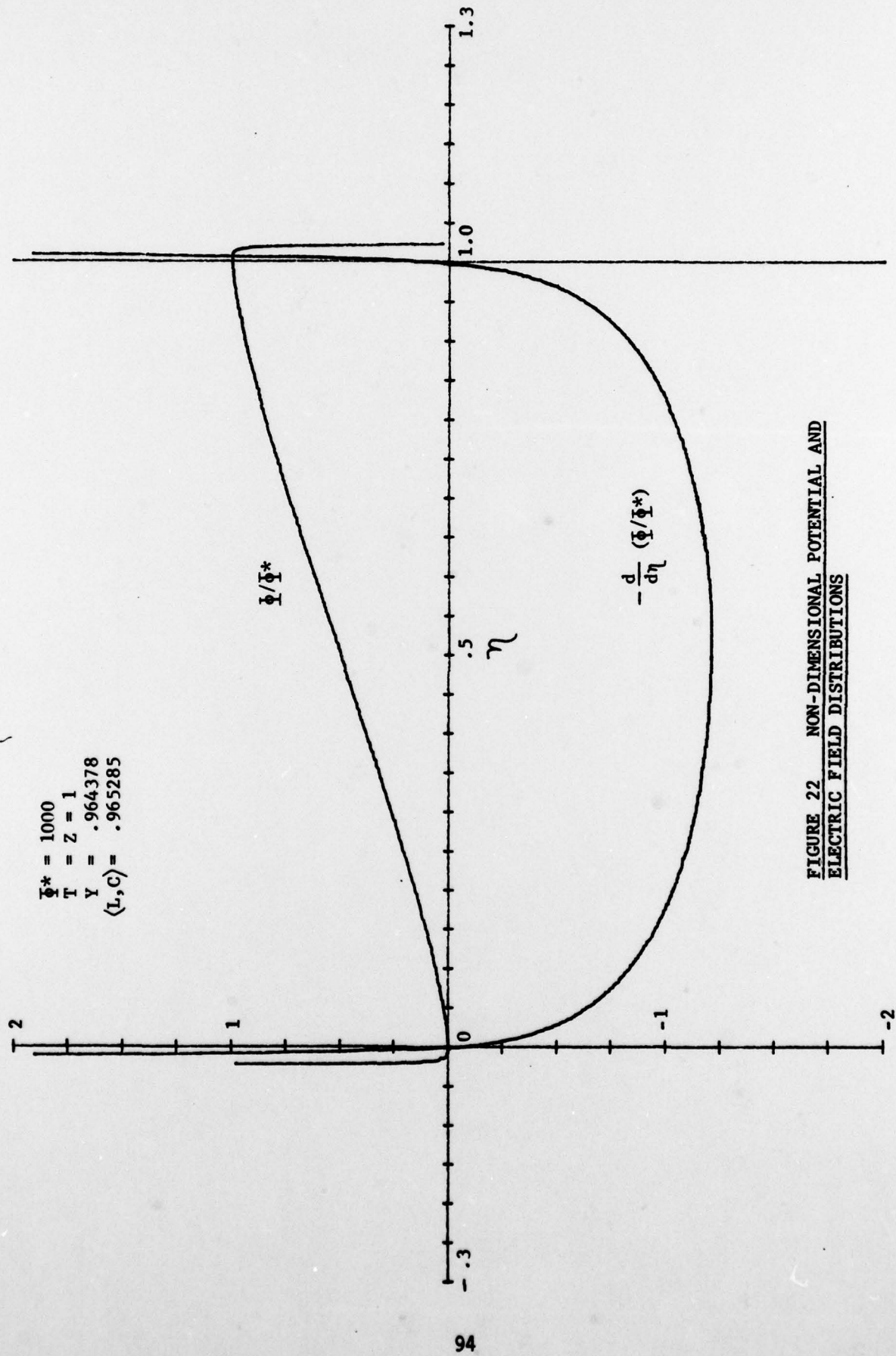Φ / Φ^*

$-\dfrac{d}{d\eta} (\Phi / \Phi^*)$

FIGURE 22   NON-DIMENSIONAL POTENTIAL AND
ELECTRIC FIELD DISTRIBUTIONS

94
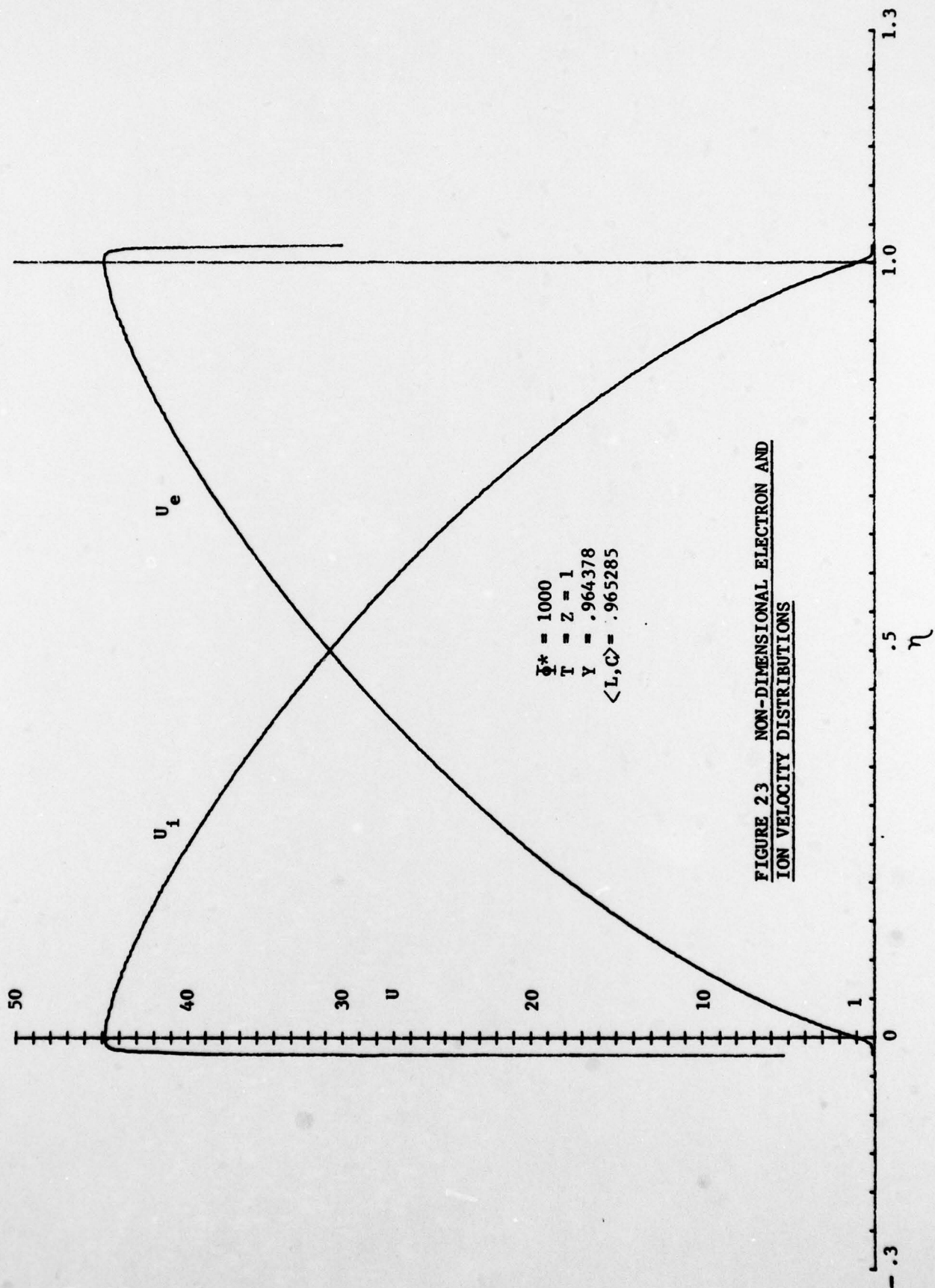
FIGURE 2 3 NON-DIMENSIONAL ELECTRON AND ION VELOCITY DISTRIBUTIONS

$\Phi^* = 1000$
$T = Z = 1$
$Y = .964378$
$\langle L, C \rangle = .965285$
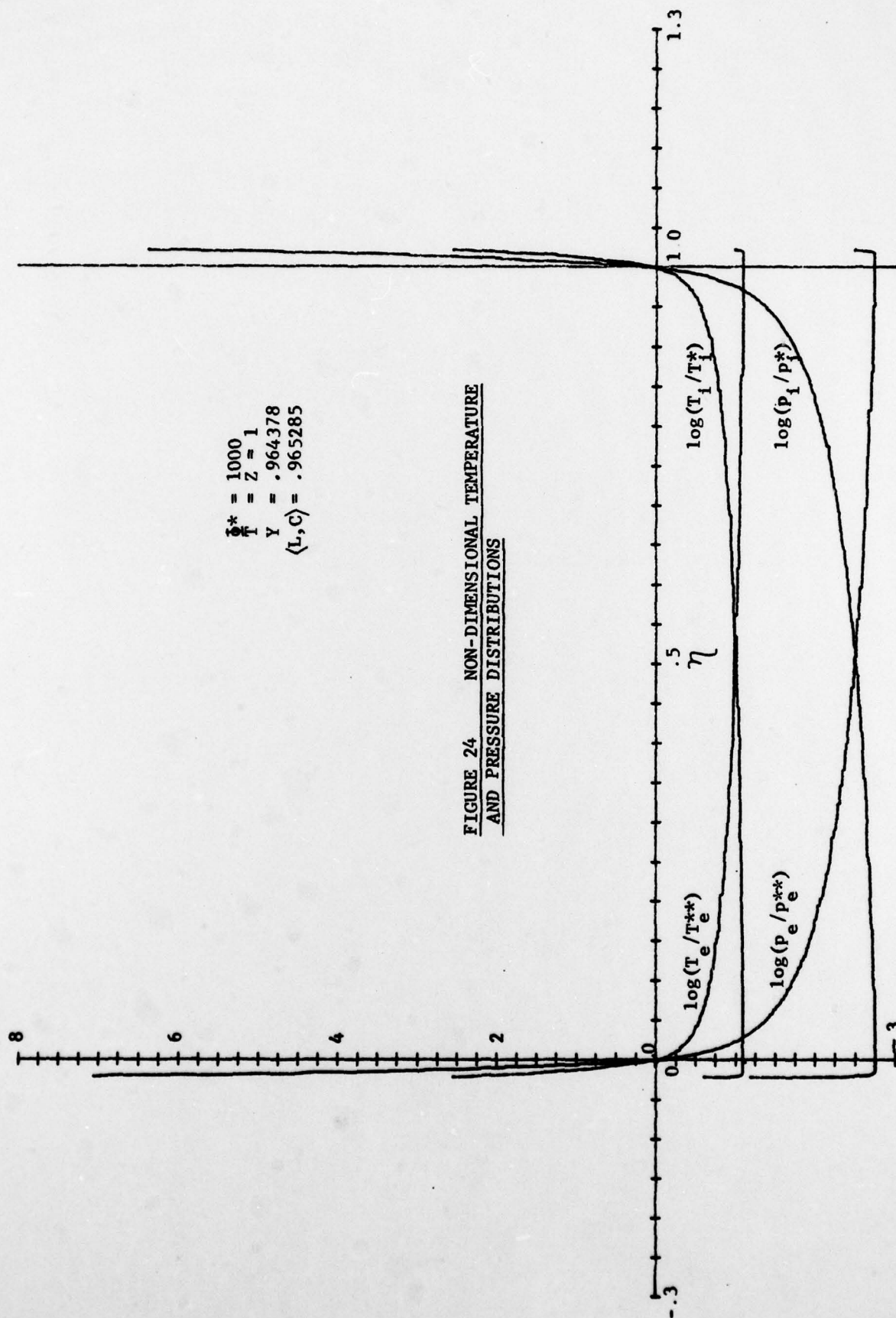
FIGURE 24   NON-DIMENSIONAL TEMPERATURE
AND PRESSURE DISTRIBUTIONS

$\Phi^* = 1000$
$T = Z = 1$
$Y = .964378$
$\langle L,C \rangle = .965285$

$\log(T_i/T_i^*)$

$\log(p_i/p_i^*)$

$\log(T_e/T_e^{**})$

$\log(p_e/p_e^{**})$

μ
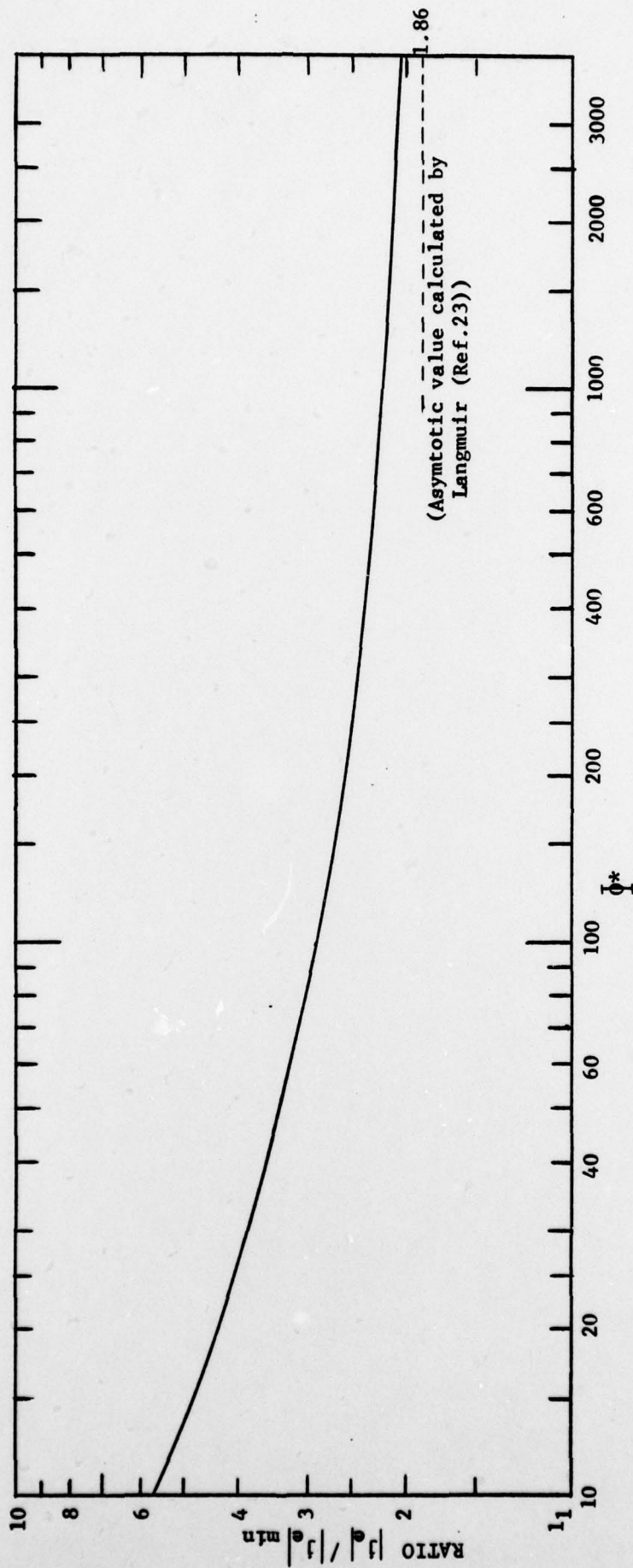
FIGURE 25   EFFECT OF ION FLOW AND POTENTIAL
DROP ON ELECTRON CURRENT DENSITY

97
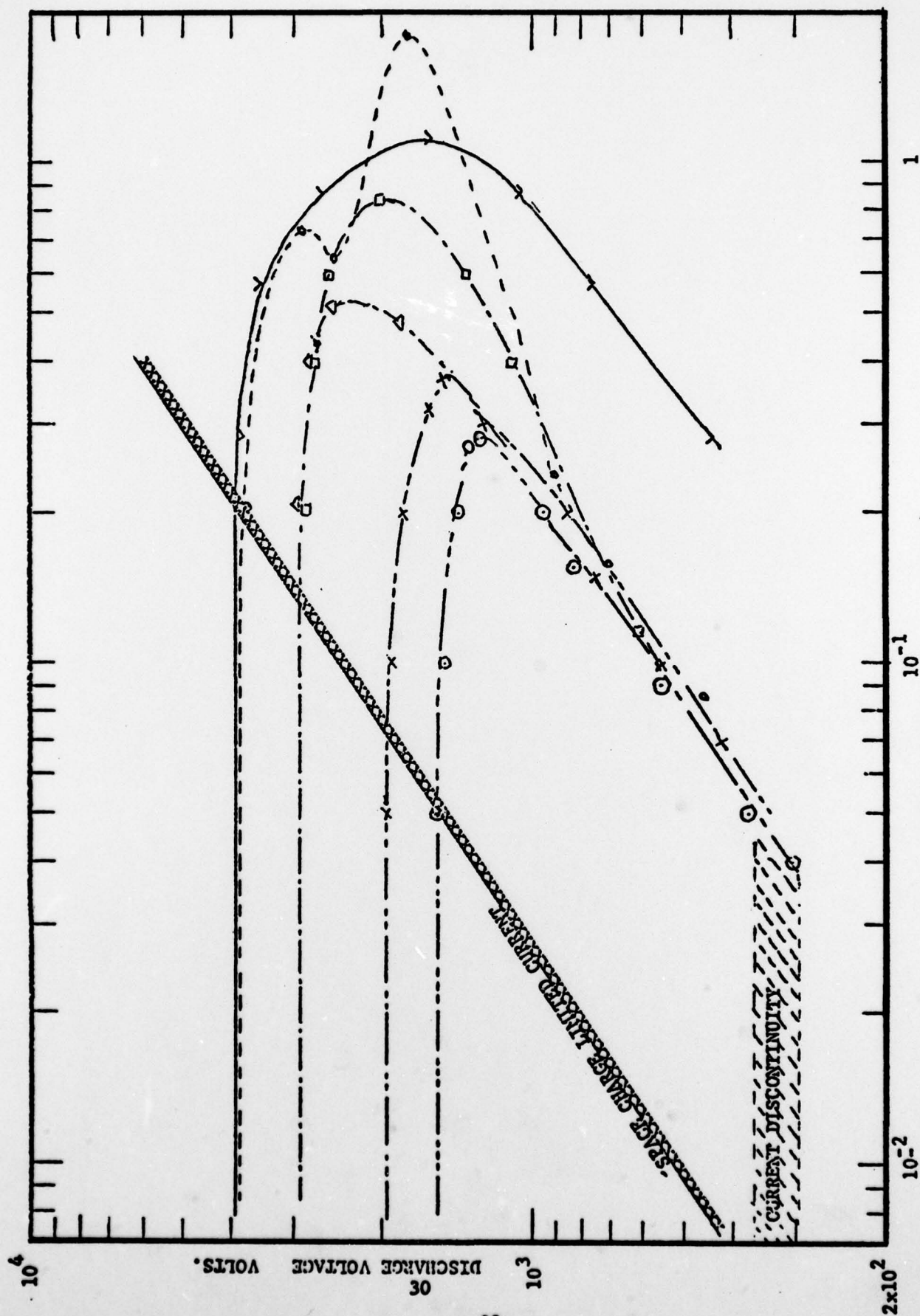
FIGURE 26. DISCHARGE CHARACTERISTICS, NO B-FIELD

DISCHARGE CURRENT (AMPERES)

DISCHARGE VOLTAGE, VOLTS.

98

DESCRIPTION
SPACE SIMULATOR, SPACECRAFT TEST LABORATORY

General Dynamics Convair Aerospace Division
San Diego, California

Internal Dimensions	Chamber "A"	12 ft. diam, 19 ft. long horizontal cylinder.
	Chamber "B"	11 ft. diam, 22 ft. long horizontal cylinder.

Pumps
Mechanical   3 to 6, 280 CFM each
Diffusion   Chamber "A" 3-15,000 l/s, mercury diffusion
                  Chamber "B" 2-95,000 l/s, oil diffusion
                               1-9500 CFM, oil diffusion (booster)
Traps   Chamber "A" -40°F freon plus LN_2 Chevron
                  Chamber "B" chilled H_2O manifold plus LN_2 Chevron
Net Speed (from chamber)   Chamber "A" 6000 l/s
                           Chamber "B" 80,000 to 95,000 l/s

Chamber Air Conditioning   500 CFM, -10°F dewpoint, 60-70°F, absolute filters.

Vacuum   Chamber "A" 1×10^{-5} Torr ultimate pressure
                  Chamber "B" $<1 \times 10^{-7}$ Torr ultimate pressure
                               with cold wall

Data   A 200 guarded-channel data system is capable of recording
                  on either or both punched tape and printed tape at 5 points
                  per second. Computers and plotters are available for data
                  reduction. Guarding and isolation of instrumentation pro-
                  vides high accuracy acquisition of millivolt signals from
                  thermocouples, etc. 100 guarded copper constantan and an
                  additional 100 copper wire passthroughs are available.

                  Thirty land lines to the Analog and Digital Computer Labora-
                  tories provide system control or additional data handling.

Location   General Dynamics Convair Aerospace, Spacecraft Test
                  Laboratory, Bldg. 28, San Diego, California, Telephone
                  277-8900, Ext. 2221.